Article

Cell Reports

Polyploid Superficial Cells that Maintain the Urothelial Barrier Are Produced via Incomplete Cytokinesis and Endoreplication

Graphical Abstract

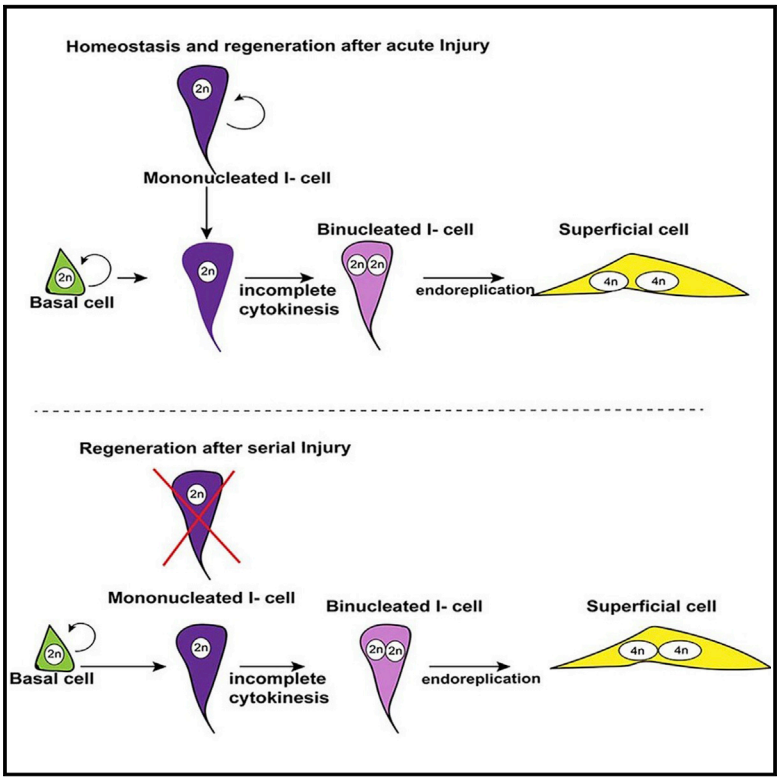

Highlights

- Binucleated S-cells are critical for maintaining the urothelial barrier
- S-cells derive from tetraploid I-cells that form via incomplete cytokinesis
- Binucleated I- and S-cells increase ploidy via endoreplication
- Polyploidy may enable the urothelium to efficiently adjust to environmental changes

Authors

Jia Wang, Ekatherina Batourina, Kerry Schneider, ..., Julie C. Canman, Indira U. Mysorekar, Cathy Lee Mendelsohn

Correspondence

clm20@cumc.columbia.edu

In Brief

Binucleated superficial cells are critical for urothelial barrier function. Wang et al. show that they derive from binucleated intermediate cells that form via incomplete cytokinesis. Both superficial and intermediate cells increase ploidy via endoreplication, a feature likely to be important for repair and response to environmental changes.

Wang et al., 2018, Cell Reports *25*, 464–477
October 9, 2018
https://doi.org/10.1016/j.celrep.2018.09.042

CellPress

OPEN ACCESS
CellPress

Cell Reports
Article

Polyploid Superficial Cells that Maintain the Urothelial Barrier Are Produced via Incomplete Cytokinesis and Endoreplication

Jia Wang,[8,9,10] Ekatherina Batourina,[4,9] Kerry Schneider,[1] Spenser Souza,[2] Theresa Swayne,[3] Chang Liu,[4] Christopher D. George,[4] Tiffany Tate,[4] Hanbin Dan,[5] Gregory Wiessner,[4] Yelena Zhuravlev,[4] Julie C. Canman,[6] Indira U. Mysorekar,[7] and Cathy Lee Mendelsohn[4,11,*]

[1]College of Veterinary Medicine, Cornell University, Ithaca, NY 14853, USA
[2]Tulane University School of Medicine, 1430 Tulane Avenue, New Orleans, LA 70112, USA
[3]Confocal and Specialized Microscopy Shared Resource, Herbert Irving Comprehensive Cancer Center, Columbia University, 1130 St. Nicholas Avenue, New York, NY 10032, USA
[4]Department of Urology, Genetics, and Development and Pathology and Cell Biology, Columbia University, 1130 St. Nicholas Avenue, New York, NY 10032, USA
[5]Department of Systems Biology, Columbia University, New York, NY 10032, USA
[6]Department of Pathology and Cell Biology, Columbia University, 630 West 168th Street, New York, NY 10032, USA
[7]Departments of Obstetrics and Gynecology and Pathology and Immunology and Center for Reproductive Sciences, Washington University School of Medicine, St. Louis, MO 63110, USA
[8]Department of Urology, Columbia University, 1130 St. Nicholas Avenue, New York, NY 10032, USA
[9]These authors contributed equally
[10]Present address: State Key Laboratory of Oncogenes and Related Genes, Renji-Med X Clinical Stem Cell Research Center, Ren Ji Hospital, School of Medicine, Shanghai Jiao, Tong University, Shanghai, China
[11]Lead Contact
*Correspondence: clm20@cumc.columbia.edu
https://doi.org/10.1016/j.celrep.2018.09.042

SUMMARY

The urothelium is an epithelia barrier lined by a luminal layer of binucleated, octoploid, superficial cells. Superficial cells are critical for production and transport of uroplakins, a family of proteins that assemble into a waterproof crystalline plaque that helps protect against infection and toxic substances. Adult urothelium is nearly quiescent, but rapidly regenerates in response to injury. Yet the mechanism by which binucleated, polyploid, superficial cells are produced remains unclear. Here, we show that superficial cells are likely to be derived from a population of binucleated intermediate cells, which are produced from mononucleated intermediate cells via incomplete cytokinesis. We show that binucleated intermediate and superficial cells increase DNA content via endoreplication, passing through S phase without entering mitosis. The urothelium can be permanently damaged by repetitive or chronic injury or disease. Identification of the mechanism by which superficial cells are produced may be important for developing strategies for urothelial repair.

INTRODUCTION

The urothelium is an epithelial barrier that extends from the renal pelvis to the bladder neck, protects against pathogens and toxins, and controls the passage of water and ions between the mucosa and underlying tissue. The adult urothelium is nearly quiescent but can quickly regenerate after acute injury from urinary tract infection (UTI) or exposure to toxins, indicating that progenitors exist in adults that are able to repair the urothelium. The mouse urothelium contains two sub-populations of basal cells (K5-basal cells and K14-basal cells), intermediate cells (I-cells), and a luminal layer lined with superficial cells (S-cells; Figure 1). S-cells are binucleated, polyploid, and post-mitotic (Hicks, 1975). They are cellular machines, specialized for synthesis and transport of Uroplakins, a family of integral membrane proteins that assemble into a crystalline apical plaque that covers most of the urothelial apical surface (Lin et al., 1994; Wu et al., 1990, 1994, 2009). S-cells connect to one another via high resistance tight junctions, forming a waterproof barrier that prevents leakage during voiding, which occurs under pressure. These cells, which can be as large as 250 μm, are able to respond to environmental cues in a number of ways. For example, during the filling phase of micturition, S-cells increase their apical surface via exocytosis of specialized fusiform vesicles that shuttle Upks to the surface, where they are assembled into uroplaque crystals. During the emptying phase of micturition, S-cells decrease their surface area via endocytosis, shuttling apical membrane/plaque into the cell for degradation (Carattino et al., 2013; Khandelwal et al., 2009; Wu et al., 2009). These specialized features likely depend on the ability of S-cells to maintain a high rate of metabolism, protein synthesis, and intracellular transport.

Variation in cell ploidy, or sets of chromosomes generated through duplication(s) of the whole genome, is a natural and important part of development in different organisms and tissues

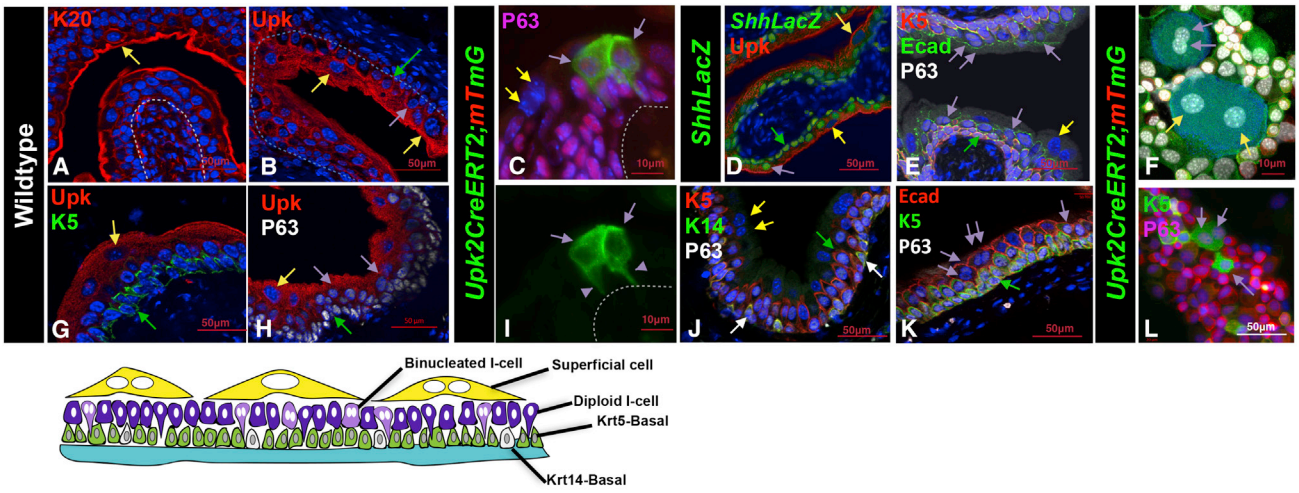

M

	Krt20	Upk	Krt5	Krt14	P63	Shh	DNA
Superficial							4n+4n
Intermediate Binucleated							2n+2n
Intermediate Mononucleated							2n
Krt14-Basal							2n
Krt5-Basal							2n

Figure 1. Identification of a New Binucleated Intermediate Cell Population Likely to Be Direct Superficial Progenitors

(A) Immunofluorescence staining shows K20 expression in sections of bladder from wild-type adult mice. The yellow arrow points to a K20-positive S-cell. Scale bar, 50 μm.

(B) Immunofluorescence staining for Upk3 in a section of bladder from a wild-type adult mouse. Scale bar, 50 μm.

(C) A cryosection from the urothelium of a *Upk2CreERT2;mTmG* mouse 10 days after tamoxifen treatment shows expression of membrane-bound *Gfp*. The purple arrows point to *Gfp*-labeled mononucleated I-cells that form very close to one another, connected to the basement membrane by thin cytoplasmic extensions (purple arrowheads in I). Scale bar, 10 μm.

(D) Immunofluorescence staining for *LacZ,* P63, and Upk in sections of a bladder from an adult *ShhLacZ* reporter mouse (Harfe et al., 2004). The yellow arrow points to a *LacZ*-negative S-cell. Purple arrows point to *LacZ*-positive intermediate cells, and the green arrow points to a *LacZ*-positive basal cell. Scale bar, 50 μm.

(E) Immunostained paraffin section from an adult wild-type mouse shows expression of K5, E-cad, and p63. The yellow arrows points to a binucleated S-cell. The double purple arrows points to binucleated I-cells. The green arrow points to a basal cell. Scale bar, 50 μm.

(F) Urothelial cells isolated from a tamoxifen-induced adult *Upk2CreERT2;mTmG* mouse. Scale bar, 10 μm.

(G) An immunostained paraffin section from a wild-type mouse shows expression of Upk and K5. The yellow arrow points to an S-cell, and the green arrow points to the K5-labeled basal cell. Scale bar, 50 μm.

(H) An immunostained paraffin section from the urothelium of an adult mouse showing expression of Upk and p63. The yellow arrow points to an S-cell; the purple arrows point to intermediate cells; and the green arrow points to a basal cell. Scale bar, 50 μm.

(I) A cryosection from the urothelium of a *Upk2CreERT2;mTmG* mouse 10 days after tamoxifen treatment shows expression of membrane-bound *Gfp*. The purple arrows point to *Gfp*-labeled mononucleated I-cells that form very close to one another and are connected to the basement membrane by thin cytoplasmic extensions. Purple arrowheads denote the *Gfp*+ cytoplasmic extensions connecting the I-cell to the basement membrane. Scale bar, 10 μm.

(J) Immunofluorescence staining for K5, K14, and p63 in sections of bladder from a wild-type adult mouse. The white arrows point to K14+ basal cells. Scale bar, 50 μm.

(K) A paraffin section from an adult mouse stained with Ecad, K5, and P63. Double purple arrowheads denote binucleated I-cells. Single purple arrow denotes a mononucleated I-cell. Scale bar, 50 μm.

(L) Cells washed from a *Upk2CreERT2;mTmG* adult mouse urothelium stained with K5 and P63. Scale bar, 50 μm.

(M) Combinatorial markers used to distinguish different urothelial populations.

across many taxa (Edgar et al., 2014; Fox and Duronio, 2013). Polyploidy has been shown to have positive features, for example, enabling cells to better respond to environmental changes or challenges, as well as negative features, including increased potential for aneuploidy, which is commonly associated with cancer and birth defects due to genome instability (Duncan et al., 2010; Losick et al., 2013; Schoenfelder and Fox, 2015; Storchova and Pellman, 2004). Besides cell-cell fusion, polyploidy can be programmed through non-canonical cell cycles, also known as endoreplication or endocycling, in which DNA replication (S phase) proceeds without intervening mitoses (Frawley and Orr-Weaver, 2015). In this case, genome duplication is uncoupled from daughter cell formation by oscillating G and S phases, as observed in plant trichromes, *Drosophila* salivary glands, and in many other fly tissues (Edgar and Orr-Weaver, 2001; Hammond and Laird, 1985; Swanhart et al., 2005). Polyploidy can also result from failed cytokinesis in which cells become binucleate (here on referred to as endomitosis), as observed in megakaryocytes, trophoblasts, hepatocytes, and *Drosophila* male accessory gland cells and larval tissues (Cao et al., 2017; Gentric and Desdouets, 2014; Nguyen and Ravid, 2010; Sarto et al., 1982; Taniguchi et al., 2014). Importantly, endomitosis and endocycling are not mutually exclusive, and both pathways for increasing genome copy number per cell have been found to occur in polyploid cells, for example, in zebrafish epicardium (Taniguchi et al., 2014).

The cellular mechanism by which S-cells achieve polyploidy is largely unexplored. Lineage studies and pulse-chase analyses suggest that both I-cells and basal cells can produce S-cell daughters depending on the conditions (Colopy et al., 2014; Gandhi et al., 2013; Papafotiou et al., 2016; Schäfer et al., 2017; Shin et al., 2011). Yet it remains unclear how binucleated polyploid S-cells are produced from mononucleated diploid populations. Here, we identify a population of binucleated I-cells that reside below the superficial layer of the urothelium that are likely to replace S-cells as they die off during homeostasis and regeneration. Using fate mapping, we show that binucleated I-cells are derived from mononucleated I-cells during urothelial homeostasis and regeneration. Using real-time imaging, we show that binucleated I-cells form via endomitosis in which diploid I-cells enter mitosis but fail to complete cytokinesis. Our studies also suggest that binucleated I- and S-cells can further increase ploidy during differentiation, via endoreplication, passing through S phase without proceeding through mitosis. Interestingly, we found that the pathway to polyploidy is likely to be conserved, regardless of which populations act as progenitors. Binucleated I-cells, are produced from a diploid I-cell population during homeostasis and after acute injury; however, diploid I-cells have a limited capacity for division and are depleted after serial or chronic injury. Under these conditions, basal cells replenish the diploid I-cell population, producing S-cells via endomitosis, thereby preserving the urothelial barrier.

RESULTS

Identification of a Binucleated Intermediate Cell Population Likely to Be Direct Superficial Progenitors

The urothelium is stratified, containing layers of basal cells, I-cells, and S-cells critical for producing and maintaining the crystalline plaque that serves as the urothelial barrier. These different populations can be distinguished by combinatorial markers (Figure 1M). Krt20 marks mature S-cells, which are also positive for Upk and negative for P63, K5, and *Shh* (Figures 1A–1H, 1J, 1L, and 1M, yellow arrows denote S-cells). I-cells co-express Upk, P63, and *Shh* and display low or undetectable expression of Krt20 and Krt5 (Figures 1b–1F, 1H, and 1K–1M, purple arrows denote I-cells). Analysis of *Upk2CreERT2;mTmG mice*, in which Gfp is localized to the cell membrane, reveals that I-cells (Gandhi et al., 2013) form very close to one another and display fine cytoplasmic projections that connect with the basement membrane (Figures 1C and 1I) The presence of these connections is likely to be important for maintaining the I-cell population, since epithelial cells require basement membrane connections in order to undergo cell division (Le Bras and Le Borgne, 2014; Oliferenko et al., 2009; Sambandamoorthy et al., 2015). The basal population contains K5-basal cells that co-express Krt5, P63, and *Shh* and exhibit low or undetectable expression of K14, Upk, or Krt20 (Figures 1B, 1D, 1E, 1G, 1H, 1J, 1K, and 1M, green arrows denote basal cells), and a second smaller population of basal cells (K14-basal cells) that express K14 as well as K5 and P63 (Figure 1J, K14 basal cells are denoted by white arrows).

Lineage studies suggest that both I-cells and Basal cells can divide and produce S-cell daughters (Colopy et al., 2014; Gandhi et al., 2013; Papafotiou et al., 2016; Schäfer et al., 2017; Shin et al., 2011). Regardless of which urothelial populations serve as progenitors, it is still unclear how S-cells, which are post-mitotic, binucleated, and polyploid, are formed from basal or I-cells, which are mononucleated and diploid. Because S-cells are post-mitotic, their binucleation is likely to occur in either basal or I-cell progenitors before they begin to differentiate into S-cells. To begin to address this, we analyzed the adult urothelium during homeostasis, when there is little, if any, proliferation, to determine whether we could detect a binucleated population of I-cells or basal cells that could be S-cell precursors. To distinguish mononucleated cells from binucleated cells, we used E-cadherin, which stains adherens junctions to visualize cell boundaries, and DAPI staining to label nuclei. Combinatorial markers were used to distinguish different urothelial sub-populations (Figure 1M). This analysis revealed a previously uncharacterized population of I-cells that are binucleated and reside just below the S-cell layer (Figures 1E and 1K, double purple arrows denote binucleated I-cells). Analysis of whole-mount preps from *Upk2CreERT2;mTmG* mice revealed that binucleated I-cells are considerably smaller than S-cells, with smaller nuclei compared to S-cells, suggesting that both cell size and DNA content change during S-cell differentiation (Figures 1F and 1L). Consistent with this, DNA content analysis by flow cytometry and Integrated DAPI fluorescence from adult urothelial samples at homeostasis, indicate that binucleated I-cells have a DNA content of about 4*n* (2*n*+2*n*) (Figure S1), half that compared to S-cells, which generally have a DNA content of 8*n* (4*n*+4*n*) (Figure S1). Based on quantification of cell numbers in paraffin-embedded tissue, binucleated I-cells account for about 11% of the total I-cell population during homeostasis, the remainder of which are mononucleated I-cells. The presence of a binucleated I-cell population that resides below the superficial layer of the

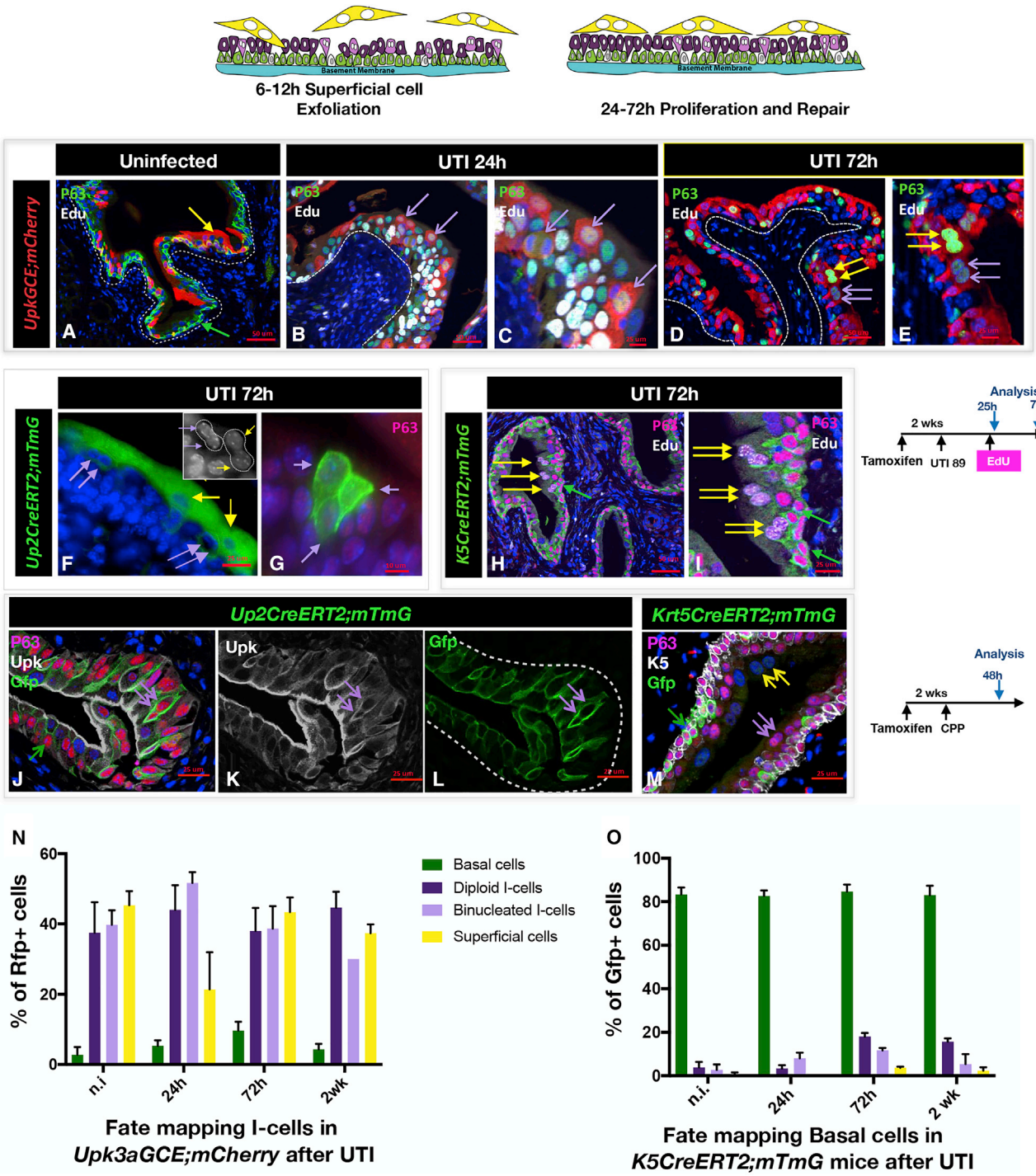

Figure 2. Binucleated I-Cells Are Produced by I-Cells after Acute Injury and Give Rise to Superficial Cells

(A) A paraffin section from an uninfected adult *Upk3aGCE;mCherry* mouse stained for expression of EdU and P63. Scale bar, 50 μm.

(B) A paraffin section from a *Upk3aGCE;mCherry* mouse 24 hr after UTI, stained for expression of *mCherry*, p63, and EdU. Purple arrows point to the *mCherry*-positive mononucleated I-cells. Scale bar, 50 μm.

(C) Same sample used in (B) but at a higher magnification.

(D) A paraffin section from a *Upk3aGCE;mCherry* mouse 72 hr after UTI stained for expression of *mCherry*, p63, and EdU. The double yellow arrows point to the *mCherry*-positive S-cells, which have been generated following UTI. The purple double arrows point to the *mCherry*-positive binucleated I-cells.

(E) Higher magnification of image in (D). Scale bar, 50 μm.

(F) A cryosection from a *Upk2CreERT2;mTmG* adult mouse 72 hr after UTI showing lineage-marked binucleated I-cells and S-cells. Scale bar, 25 μm.

(legend continued on next page)

urothelium suggests that these cells may be progenitors that can quickly replace S-cells upon injury, thereby preserving the urothelial barrier.

Diploid I-Cells Produce Binucleated I-Cells and S-Cells after Injury

The existence of a newly identified binucleated I-cell sub-population, raises the possibility that these are direct S-cell progenitors. Recent studies suggest that both I-cells and basal cells can contribute to the S-cell population, depending on the extent of urothelial injury (Schäfer et al., 2017). To determine which populations produce binucleated I-cells, we performed fate-mapping experiments using the *Upk3aGCE;mCherry* and *Krt5CreERT2;mTmG* mice to label I-cells and basal cells, respectively, and then we compared their respective contributions to different urothelial sub-populations after regeneration in response to acute injury. We first used UTI, a well-studied model of acute injury and repair (Hung et al., 2009), to induce regeneration. For these experiments, females received a transurethral inoculation of UTI 89, a strain of Uropathogenic *E. coli* (UPEC) isolated from a patient with cystitis (Garofalo et al., 2007). UPEC infects S-cells and establishes intracellular bacterial communities 6- and 12-hr post-infection (p.i.) (Figure S2A, white arrows). UPEC infected S-cells subsequently undergo exfoliation, which occurs between 6- and 12-hr post-inoculation (Figure S2B; arrows denote exfoliating S-cells). Basal and I-cells survive UTI and undergo a burst of cell-cycle activity 24 hr p.i., evidenced by expression of Ki67 and EdU, which is taken up during S phase, markers that are rarely detectable in the homeostatic urothelium, which is virtually quiescent (Jost, 1986; Jost and Potten, 1986) (Figures 2A–2E, 2H, 2I, S2D, and S2E). A new S-cell layer is established by 72-hr p.i. and regeneration is complete 2 weeks after infection when Krt20 expression is restored in the S-cell layer (Figure S2C).

The *Upk3aGCE;mCherry* line has a labeling efficiency of about 56%, and Cre-dependent recombination will label I-cells and their daughters with *mCherry* (Gandhi et al., 2013; Van Batavia et al., 2014). Analysis of *Upk3aGCE;mCherry* mice between 24 hr and 2 weeks p.i. revealed *mCherry* expression labeling 44% of mononucleated I -cells and 51% of the binucleated I-cell population 24 hr after infection, 43% of S-cells by 72 hr, as well as a small number (5%) of basal cells (Figures 2A–2E, 2N, and S2F–S2I). Importantly, we identified clones containing lineage-marked binucleated I-cells situated just below a lineage-marked binucleated S-cell, as well as clones containing two diploid I-cell and two likely daughters (Figures 2F and 2G), suggesting that I-cells can produce a binucleated population as well as divide, and produce diploid I-cells. Similar findings were observed using the Cyclophosphamide (CPP) model to induce a single round of regeneration. In this case, we used the *Up2CreERT2;mTmG* line, which has a labeling efficiency of 89% to mark I-cells and their daughters, and we analyzed the distribution of lineage-marked (*Gfp*+) diploid (mononucleated) I-cells, binucleated I- and S-cells 48 hr after CPP treatment, when proliferation peaks (Figures 2J, 2K, and S2N–S2U). These studies revealed *Gfp* labeling in 73% of I-cells and binucleated I-cells, and 87% of S-cells (Figure 5A), supporting the idea that I-cells produce binuclear I- and S-cells after acute injury.

To examine whether basal cells also contribute to the I- or S-cell populations, we used the *Krt5CreERT2;mTmG* line, which has a labeling efficiency of about 84%, to follow the fate of basal cells during regeneration. Analysis of the distribution of *Gfp*+ cells in *Krt5CreERT2;mTmG* mice 24 hr after UTI revealed extensive labeling (greater than 80%) in the basal population as well as 3% of mononucleated I-cells and 8% of binucleated I-cells, while analysis at 72 hr when newly formed S-cells are present, revealed labeling in 3% of the S-cell population (Figure S2O). These observations indicate that basal cells contribute to the I-cell population. Analysis of regeneration in *Krt5CreERT2;mTmG* mice using the CPP model of injury and repair revealed a higher rate of contribution to the I- and S-cell lineages. In this case, about 20% of the diploid I-cell population were lineage marked, as well as, 16% of the binucleated I-cell population and 7.5% of the S-cell population after 1X CPP (Figures 2M and 5B). Together, these studies suggest that I-cells are able to divide and to produce binucleated I- and S-cell daughters after acute injury, while K5-basal cells can contribute to the I-cell population after UTI, but make a more significant contribution to the I-cell population after CPP. These findings also raise the possibility that the UTI and CPP injury models affect the behavior of basal and I-cell progenitors differently.

Binucleated I-Cells Form via Endomitosis

Binucleated cells can be produced by cell fusion of mononucleated cells or by endomitosis, in which cells progress partway through mitosis, but fail to complete cytokinesis and daughter cell separation (Duncan et al., 2010; Fortier et al., 2017; DePamphilis, 2016; Rios et al., 2016). If binucleated I-cells are produced by cell fusion, we would expect nuclei to be derived from two different mononucleated I-cells, and hence distributed randomly. Whereas, if binucleated cells arise via endomitosis, we expect that both nuclei would be derived from the same I-cell of origin. To distinguish between these possibilities, we

(G) A cryosection from a *Upk2CreERT2;mTmG* adult mouse 72 hr p.i. stained with P63 shows a clone of mononucleated I-cells. Scale bar, 10 μm.
(H) A paraffin section from an adult *K5CreER;mTmG* mouse 72 hr after UTI stained for expression of *Gfp*, P63, and EdU. The double yellow arrows point to *Gfp*-negative S-cells. Scale bar, 50 μm.
(I) Same sample used in (B) but at a higher magnification.
(J) A paraffin section isolated from a CPP-treated adult *Upk2CreERT2;mTmG* mouse 48 hr after CPP treatment, stained with P63, Upk, and Gfp. Scale bar, 25 μm.
(K) Same sample used in (J) but showing Upk expression. The double purple arrows point to a binucleated I-cell expressing *Gfp*. Scale bar, 25 μm.
(L) Same sample used in (J) but showing Gfp expression.
(M) A section from a *K5CreER;mTmG* mouse 48 hr after administration of CPP and stained with P63 and K5. Scale bar, 25 μm.
(N) Quantification of lineage-marked urothelial populations at different stages after UTI in *Upk3aGCE;Rfp* mice. For quantification, a minimum of three independent experiments were performed, and numbers are means of percentages ± SEM.
(O) Quantification of lineage-marked urothelial populations at different stages after UTI in *K5CreER;mTmG* mice.

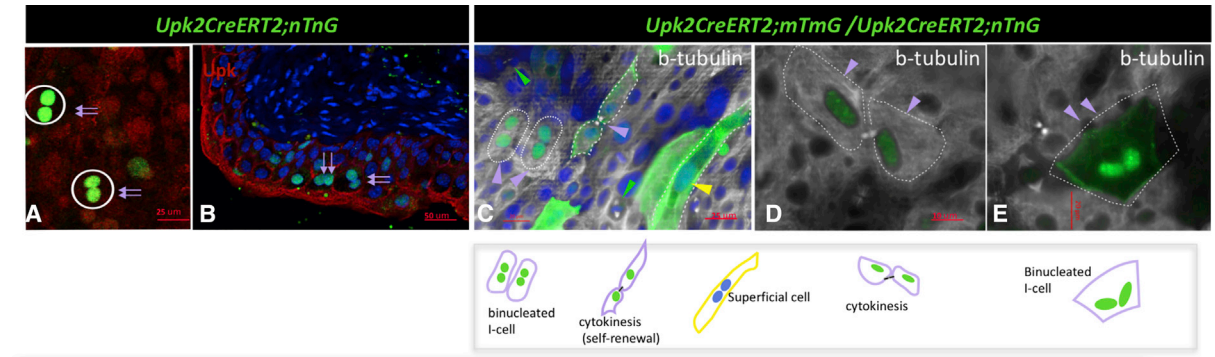

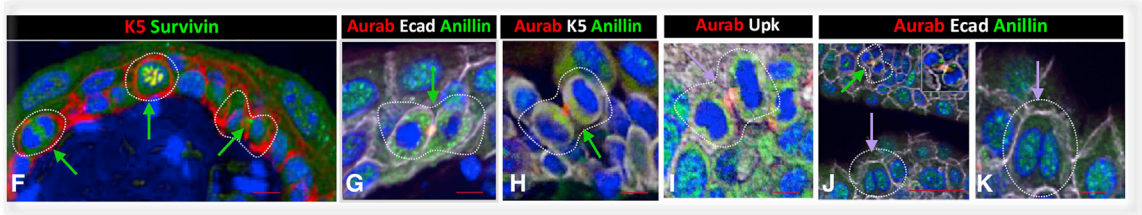

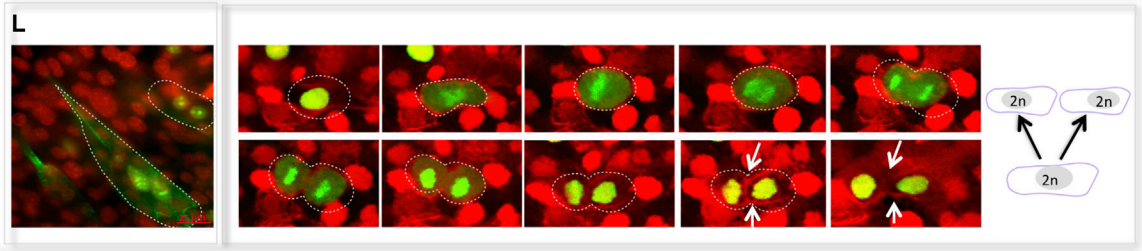

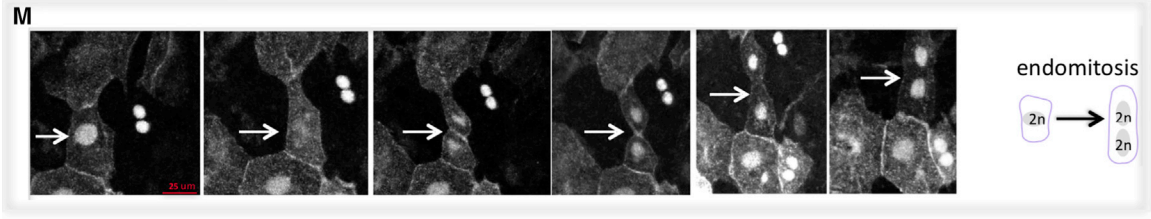

N Basal cells and l-cells divide after injury induced by UTI

	Intermediate Cells			Basal Cells		
	Cytokinesis Events	Total # cells	Percentage	Cytokinesis Events	Total # cells	Percentage
UTI 24h n=5	31	792	3.9%	37	1152	3.2%
UTI 36h n=3	20	728	2.7%	25	1694	1.5%
UTI 48h n=3	14	213	6.5%	2	304	0.7%

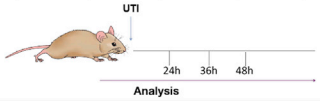

O Basal cells and l-cells divide after injury induced by CPP

	Intermediate Cells			Basal Cells		
	Cytokinesis Events	Total # cells	Percentage	Cytokinesis Events	Total # cells	Percentage
CPP 48h n=3	8	2261	0.4%	64	8422	0.7%
CPP 52-55h n=2	8	270	3.0%	7	1812	0.4%
CPP 60h n=4	38	1526	2.5%	72	4995	1.4%
CPP 72h n=2	6	678	0.9%	5	1109	0.5%

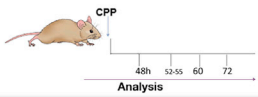

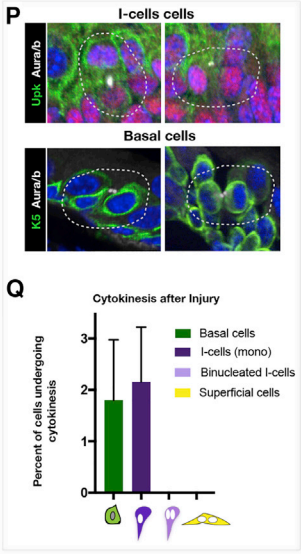

(legend on next page)

performed fate mapping using *Upk2CreERT2;nTnG* mice. In this line, cells that undergo Cre-dependent recombination express nuclear *Gfp* and in cells that have not undergone recombination, nuclei are *Tomato* positive (Figure 3A). *Upk2CreERT2;nTnG* mice were treated with tamoxifen to induce recombination, infected with UPEC 2 weeks later, then analyzed 24- or 72-hr p.i. to evaluate the distribution of nuclear *Gfp* and *Tomato*. This analysis revealed 522/522 instances in which both nuclei were *Gfp*+, Tomato+, or negative for both markers and no instances in which marker expression was in one nucleus, but not the other (Figure 3B), strongly suggesting that binucleation occurs via a mechanism other than cell fusion.

The failure to observe evidence of mononucleated I-cell fusion after UTI suggests that binucleated I-cells form via endomitosis, entering the cell cycle, and exiting mitosis prior to completing cytokinesis. To begin to investigate how binucleation occurs, we analyzed sections of urothelium from wild-type adult mice 24 hr after infection with UPEC to identify mitotic cells and binucleated cells that are likely products of endomitosis. Urothelial sections were stained for expression of mitotic markers including aurora B kinase, survivin, and anillin. Aurora B and survivin, which are components of the chromosome passenger complex (CPC), localize to the nucleus and centromeres during early mitosis and to the central spindle and cell cortex during cytokinesis (Caldas et al., 2005; Carmena and Earnshaw, 2003). Anillin accumulates at the contractile ring and midbody in late anaphase or telophase during cytokinesis and is localized in the nucleus in late G1, G2, and S phases (Field and Alberts, 1995). These analyses revealed K5-basal cells in all phases of the cell cycle (Figures 3F–3H and 3J, green arrows point to mitotic basal cells). We observed I-cells expressing anillin and aurora B that were in late telophase or had undergone normal cytokinesis (Figures 3I–3K). This analysis also revealed binucleated I-cells with nuclear expression of Anillin and undetectable expression of aurora B/survivin, indicating that these cells are in interphase rather than in mitosis and hence likely to be products of endomitosis (Figures 3E, 3J, 3K, 3N, 3R, and 3S). The observation that similar proportions of basal and diploid I-cells were in cytokinesis (1.8% and 2.2%, respectively; Figures 3N–3P), suggests that both populations divide during regeneration (Figures 3N, 3P, and 3Q).

Taken together, our findings suggest that basal cells divide and produce a diploid I-cells, which differentiate into S-cell daughters after acute injury, whereas diploid I-cells divide and produce binucleated I- and S-cell daughters by endomitosis. To directly address this question, we used lineage tracing to mark I-cells and then we examined their behavior during mitosis using real-time imaging and an organotypic culture system developed in the lab (Batourina et al., 2012). Thick sections (0.3 to 0.5 cm in size) containing urothelium and associated stroma were placed in culture where they undergo a period of regeneration that lasts about 7 days, followed by a period of quiescence, which can be maintained for up to 1 month. In control experiments, we first compared the urothelium in organotypic cultures during the period of proliferation with *in vivo* samples of regenerating urothelium, using the *Upk3aGCE;mCherry* line in both cases to lineage mark I-cells (Figures S3A–S3H). For *in vivo* lineage tracing, *Upk3aGCE;mCherry* mice were injected with tamoxifen to induce recombination, infected with UPEC, then treated with EdU 24 hr after infection to label cells in S phase, which are exceedingly rare in the urothelium during homeostasis. For *in vitro* analysis, explants from *Upk3aGCE;mCherry* mice were cultured for 3 days, treated with 4-OHT to induce recombination and analyzed 2 days later to compare the distribution of lineage-marked cells *in vitro* and *in vivo*. Analysis of tissue from *in vivo* samples of urothelium revealed

Figure 3. Binucleated I-Cells Form via Endomitosis

(A) Nuclear *Gfp* and Tomato expression in a whole-mount preparation from a *Up2CreERT2;nTnG* mouse. Scale bar, 25 μm.

(B) A section from a *Up2CreERT2;nTnG* mouse 24 hr after UTI shows binucleated *Gfp*+ I-cells (purple arrows). Scale bar, 50 μm.

(C) Whole-mount prep of urothelium from an adult *Up2CreERT2;mTmG;nTnG* mouse isolated 24 hr after UTI and stained with beta-tubulin showing membrane-bound Gfp in an I-cell that has divided and in an S-cell (purple and green arrowheads), as well as an unlabeled basal cell which is dividing.

(D) Whole-mount prep of urothelium from an adult *Up2CreERT2;mTmG;nTnG* mouse isolated 24 hr after UTI and stained with beta-tubulin showing a pair of I-cells that have undergone cytokinesis.

(E) Whole-mount prep of urothelium from an adult *Up2CreERT2;mTmG;nTnG* mouse isolated 24 hr after UTI and stained with beta-tubulin showing membrane and nuclear Gfp staining in a binucleated I-cell, which is negative for b-tubulin expression and is therefore likely to be a produce of incomplete cytokinesis. Yellow arrowheads denote S-cells, purple arrowheads deonote I-cells and green arrowheads denote Basal cells.

(F) A paraffin section from a CPP-treated wild-type mouse 48 hr after CPP treatment, stained for K5 and Survivin expression. Scale bar, 25 μm.

(G) A paraffin section from a CPP-treated wild-type mouse 48 hr after CPP treatment, stained for Ecad anillin and Aura/b expression. Scale bar, 25 μm.

(H) A paraffin section from a CPP-treated wild-type mouse 48 hr after CPP treatment, stained for K5, anillin, and Aura/b expression. Scale bar, 25 μm.

(I) A paraffin section from a CPP-treated wild-type mouse 48 hr after CPP treatment, stained for Upk and Aura/b expression. Scale bar, 25 μm.

(J) A paraffin section from a CPP-treated wild-type mouse 48 hr after CPP treatment, stained for Ecad, anillin, and Aura/b expression. Scale 50 μm.

(K) Same sample used in (J) but at a higher magnification. The purple arrow points to a binucleated I-cell that is not expressing mitotic markers. Scale bar, 10 μm.

(L) A whole-mount preparation from a cultured *Up2CreERT2;mTmG;nTnG* mouse urothelium showing lineage-marked binucleated I-cells and S-cells and a series of images from a real-time video of cultured urothelium and stroma from a *Up2CreERT2;mTmG;nTnG* mouse showing an I-cell undergoing normal cytokinesis. White arrow points to the cleavage furrow. Scale bar, 25 μm.

(M) A series of images from a real-time move of cultured urothelium and stroma from a *Up2CreERT2;mTmG;nTnG* mouse undergoing endomitosis. The white arrows point to the cleavage furrow, which forms and then regresses. Scale bar, 25 μm.

(N) Quantitation of cytokinetic events in I-cells and basal cells after UTI.

(O) Quantitation of cytokinetic events in I-cells and basal cells after injury and regeneration induced by CPP.

(P) Images showing examples of I-cells and basal cells stained with Aura/b, showing cells undergoing cytokinesis.

(Q) Comparison of cytokinetic events in basal cells, mononuclear I-cells, binuclear I-cells, and S-cells after injury. For quantification, a minimum of three independent experiments were performed, and numbers are means of percentages ± SEM.

mCherry expression restricted to mononuclear and binucleated I- and S-cells, as expected, whereas basal cells were unlabeled (Figures S3A, S3B, S3E, and S3F). Analysis of cultured urothelium revealed remarkable preservation of urothelial stratification and sub-populations. We observed mononucleated and binucleated I-cells and S-cells co-labeled with *mCherry* and EdU (Figures S3C, S3D, S3G, and S3H) and unlabeled K5-basal cells that were EdU positive (Figure S3C). These observations suggest that the culture model effectively maintains urothelial proliferation, stratification, and differentiation and can be used to analyze urothelial regeneration *in vitro*.

To visualize the mitotic behavior of I-cells *in vitro*, we generated a lineage-model in which I-cell nuclei and cell membranes can be simultaneous visualized by intercrossing *Upk2CreERT2;mTmG* mice with *UpkCreERT2;nTnG* mice. Cre-dependent recombination induces expression of membrane-bound *Gfp* in *Upk2CreERT2;mTmG* mice, and nuclear *Gfp* in *UpkCreERT2;nTnG* mice (Figures 3C, 3D, and 3L). Analysis of whole-mount urothelium isolated from *Up2CreERT2;mTmG;nTnG* mice 24 hr after UTI revealed beta-tubulin expression in *Gfp*-positive mononucleated I-cells that were undergoing cytokinesis (Figures 3C and 3D, purple arrowheads) as well as in binucleated I- and S-cells, which were negative for beta-tubulin and presumably post-mitotic (Figures 3C–3E, purple arrowheads denote binucleated I-cells expressing nuclear *Gfp*, yellow arrowhead denotes a S-cell expressing membrane-bound *Gfp*). Thus, we distinguished between lineage-marked diploid and binucleated I-cells using this system.

To directly visualize the behavior of I-cells during regeneration, we performed real-time imaging of organotypic cultures. Explants from *Up2CreERT2;mTmG;nTnG* mice were maintained for 3 days in culture then treated with 4-OHT to induce recombination and placed on a stage-top incubator. Multiphoton confocal images were collected every 5 min for 24 hr to produce real-time videos. Representative image sequences are shown in Figures 3L and 3M. We observed four instances in which I-cells underwent apparently normal cell division, passing through the regular stages of mitosis and cytokinesis (Figure 3L; Video S1). We also observed three instances in which I-cells undergoing endomitosis, progressing through mitosis and forming a cytokinetic furrow that subsequently regressed (Figure 3M; Video S2). Normal cytokinesis lasted 2–3 hr, whereas endomitosis lasted up to 7 hr. Importantly, we did not observe evidence of I- or S-cells fusing in these experiments, nor did we observe binucleated I- or S-cells undergoing cytokinesis after injury (Figure 3Q), suggesting that S-cells, which have twice the DNA content compared to binucleated I-cells can increase their DNA content without entering mitosis.

Binucleated I-Cells Increase Ploidy as They Differentiate into S-Cells via Endoreplication, Entering S Phase without Passing through Mitosis

S-cells have two nuclei, a total DNA content equivalent to 8*n* (4*n*+4*n*) or higher (Stewart, 1986), and are considered to be post-mitotic (Jost, 1986). Next, we sought to address how S-cells attain a DNA content twice that of binucleated (2*n*+2*n*) I-cells. To evaluate whether this ploidy increase is associated with cell division of binucleated I or S-cells, we first analyzed the distribution of aurora B, survivin, and anillin, to label dividing cells in wild-type urothelium after UTI. This analysis revealed 0/927 instances of binucleated I-cells in mitosis/cytokinesis and 0/4,163 instances of S-cells in mitosis/cytokinesis, suggesting that the ploidy increase in S-cells is not associated with cell division of either precursor cell type (Figure 4I). Since we have not observed evidence for fusion or expression of cell division markers, these observations suggest that binucleated I and/or S-cells likely undergo endocycling, entering S phase without completing mitosis (Duncan et al., 2010; Fortier et al., 2017; DePamphilis, 2016; Rios et al., 2016).

To investigate S-cell endocycling more directly, we performed pulse-chase experiments to visualize the ontogeny of 8*n* S-cells during regeneration induced by CPP and UTI. For CPP-induced regeneration, animals were treated with CPP and exposed to a 1-hr pulse of EdU either at 48 hr, when proliferation peaks, or at 72 hr, when S-cells are forming in the luminal layer. Importantly, we did not detect EdU uptake in the non-injured homeostatic urothelium (Figures 4A, 4D, and 4I), which has an extremely slow rate of cell turnover. Representative samples analyzed 48- or 72-hr post-CPP reveal EdU-positive binucleated I-cells and S-cells (Figures 4B, 4C, 4E, and 4F), suggesting both of these polyploid cells are able to enter S phase. Analysis of the urothelium during regeneration induced by UTI, revealed similar findings: EdU-labeled binucleated I-cells and S-cells were observed after a 1-hr EdU pulse at 24 hr, with the peak of proliferation at 72 hr when S-cells are replenished in the luminal layer (Figures 4G and 4H), suggesting that these polyploid cells are likely to be in S phase. Quantification after UTI and CPP revealed EdU expression in 12% of binucleated I-cells and 17.5% of S-cells, suggesting that both cell types have the capacity to enter S phase (Figure 4J). Together, the absence of mitotic markers in binucleated I- and S-cells suggests that both cell types increase ploidy through endocycling.

Basal Cells Produce Diploid and Binucleated I-Cell Daughters after Serial Injury and Repair

Our previous studies and results shown here suggest that I-cells undergo normal cytokinesis and produce binucleated I- and S-cells after acute injury. Recently published work, comparing the regenerative potential of I and basal cells in surgical models of bladder augmentation indicates that both I and basal cells contribute to repair after focal injury, whereas only basal cells have the capacity to generate urothelial cells *de novo*, which populate acellular grafts (Schäfer et al., 2017), suggesting that different types of bladder injury may favor different progenitor populations. Further support for this idea comes from studies indicating that basal cells serve as the major urothelial progenitors both after acute and serial injury induced by high doses of Cyclophosphamide (Papafotiou et al., 2016), a drug used to treat cancer that can cause cystitis (Cox, 1979; Vasconcelos-Nóbrega et al., 2012). Thus, we tested whether serial injury changes the behavior of I or basal cells during regeneration. We used the *K5CreERT2;mTmG* line to label K5-basal cells and their daughters, and the *Up2CreERT2;mTmG* line to mark I-cells and their daughters and then compared their respective regenerative capacities after a single round of

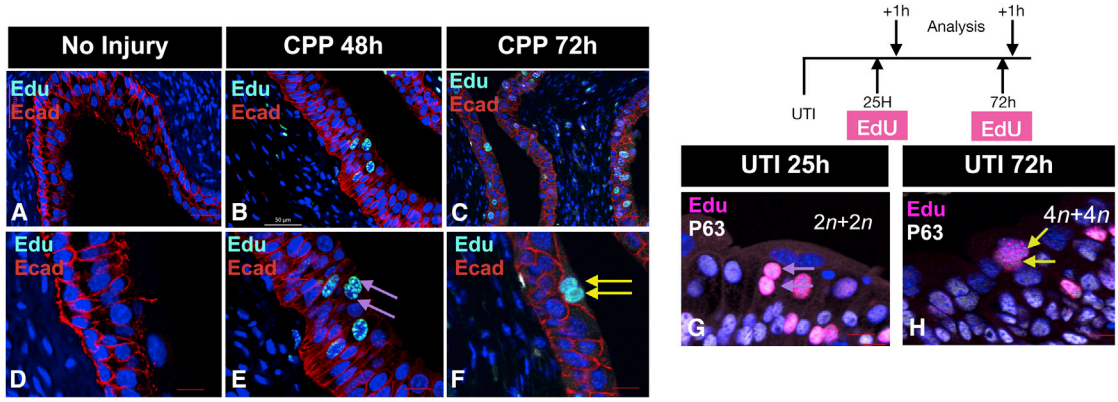

I

BINUCLEATED I-CELLS AND SUPERFICIAL CELLS DON'T UNDERGO CYTOKINESIS					
Superficial cells			Binucleated I-cells		
Control	CPP	UTI	Control	CPP	UTI
1624	1435	1104	296	215	416
0	0	0	0	0	0
n=3	n=9	n=18	n=2	n=3	n=5
TOTAL=0/4163			TOTAL=0/927		

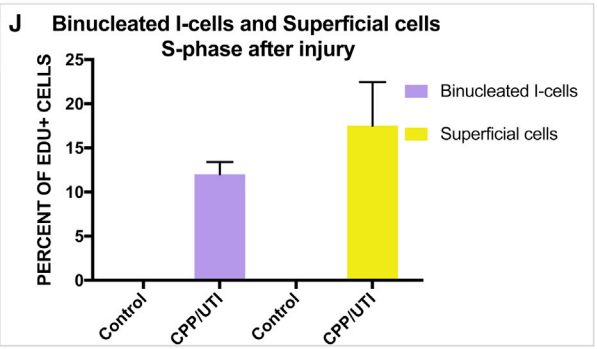

Figure 4. Binucleated I-Cells and S-Cells Are Likely to Increase Ploidy by Endocycling

(A) A section from the urothelium of an untreated adult mouse stained for expression of Ecad and EdU. Scale bar, 50 μm.

(B) A section from an adult mouse 48 hr after CPP, given a 1-hr pulse of EdU stained for EdU and Ecad. Note EdU-expressing binucleated I-cells, which are likely to be in S phase. Scale bar, 50 μm.

(C) A section from an adult mouse 72 hr after CPP, given a 1-hr pulse of EdU prior to sacrifice stained for expression of Ecad and EdU. Note EdU-expressing S-cells, which are likely to be in S phase. Scale bar, 50 μm.

(D) Same sample used in (A) but at a higher magnification.

(E) Same sample used in (B) but at a higher magnification.

(F) Same sample used in (C) but at a higher magnification.

(G) A paraffin stained section from an adult mouse 24 hr p.i. analyzed 1 hr after a pulse of EdU and stained for EdU and P63 expression. Scale bar, 25 μm.

(H) A paraffin-stained section from an adult mouse 72 hr p.i. analyzed 1 hr after a pulse of EdU and stained for EdU and P63 expression. Scale bar, 25 μm.

(I) A table showing a summary of quantification of binucleated I-cells and S-cells in cytokinesis.

(J) A bar graph showing the percentage of EdU+ binucleated I-cells and S-cells after a 1-hr pulse, which are likely to be in S phase, in animals 24–72 hr after UTI and CPP-induced injury and repair.

CPP, or after five rounds of CPP. *K5CreERT2;mTmG* and *Up2CreERT2;mTmG* mice were treated with tamoxifen to induce recombination and injected with CPP 2 weeks later. For a single round of injury, animals were treated with CPP and analyzed 2 weeks after CPP administration. For chronic injury, animals were given five doses of CPP with 2 weeks in between each dose and analyzed after the last CPP injection (Figure 5). Analysis of *Upk2CreERT2;mTmG* mice after one round of CPP revealed *Gfp* expression confined to the I- and the S-cell compartments, labeling 73% of mononucleated I-cells, 73% of binucleated I-cells, and 87% of S-cells (Figures 5A, 5C, and 5D). After five rounds of CPP, however, *Gfp*-labeling was present in only 9% of I-cells, 8% of binucleated I-cells and 20% of S-cells (Figure 5A, bottom panel; Figures 5I and 5J), suggesting that the I-cell population was exhausted after chronic injury and no longer contributes to the regenerative process.

Analysis of *K5CreERT2;mTmG* mice after one round of CPP-induced injury and regeneration revealed *Gfp* labeling in 24% of I-cells, 16% of binucleated I-cells and 7% of S-cells (Figure 5B, top panel; Figures 5E and 5F), while after five rounds of CPP, 86% of mononucleated I-cell population, 84% of binucleated I-cells and 87% of S-cells expressed the *Gfp* lineage mark (Figure 5B, bottom panel; Figures 5K and 5L). Together, these findings suggest that I-cells are likely to divide and produce binucleated I-cells and S-cells during homeostasis and after acute injury. On the other hand, basal cells produce a fraction of I-cells during regeneration following acute injury, whereas, after serial injury, basal cells are the progenitor population that repairs the urothelium. Interestingly, histological analysis and analysis for expression of leukocyte markers, reveals significant inflammation in the urothelium after five rounds of CPP, which is not observed after one round of CPP (Figures 5G, 5H, 5M, and

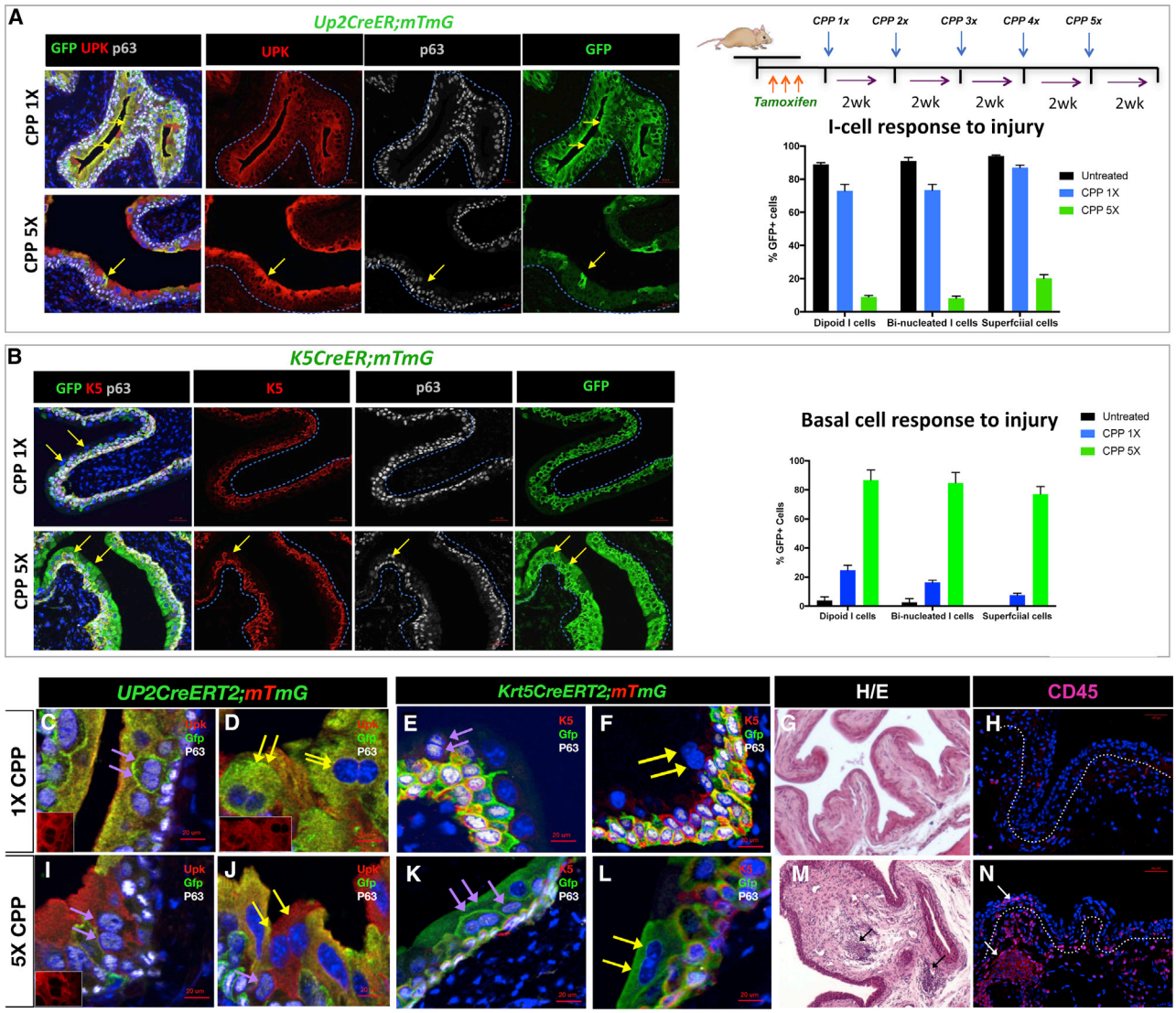

Figure 5. S-Cells Are Generated from Either I or Basal Cells during Regeneration, Depending on the Extent of Injury

(A) Paraffin sections of bladders isolated from *Up2CreERT2;mTmG* mice after one or five rounds of CPP-induced injury and regeneration. The yellow arrows point to lineage-marked S-cells. Sections were stained for expression of *Gfp*, Upk, and P63. Scale bar, 50 μm. The right-top panel shows a schematic description of the injury model. The graph shows the distribution of *Gfp*-expression in mononucleated I-cells, binucleated I-cells, and S-cells in *Up2CreERT2;mTmG* that were untreated, treated 1× with CPP, and after 5× CPP treatment.

(B) Paraffin sections from *K5CreER;mTmG* after one or five rounds of CPP-induced injury and regeneration. Sections were stained for expression of *Gfp*, K5, and p63. Scale bar, 50 μm. The graph in the right panel shows the distribution of *Gfp*-expression in mononucleated I-cells, binucleated I-cells, and S-cells in untreated *K5CreER;mTmG* mice and in *K5CreER;mTmG* mice after 1× CPP and 5× CPP treatment. Scale bar, 50 μm.

(C) A section from a *Up2CreERT2;mTmG* mouse treated 1× with CPP showing lineage-marked binucleated I cells (purple arrows). Inset shows Upk expression in a low power magnification of the same section.

(D) A section from a *Up2CreERT2;mTmG* mouse treated 1× with CPP showing lineage-marked S-cells (yellow arrows). Inset is Upk staining alone in a lower magnification image of the same section.

(E) A section from a *Krt5CreERT2mTmG* mouse after 1 round of CPP showing lineage-marked basal cells as well as a binucleated I cell that is unlabeled (purple arrows).

(F) A section from a *Krt5CreERT2mTmG* mouse after 1 round of CPP showing Gfp-labeled basal cells as well as a binucleated S cell that is unlabeled (yellow arrows).

(G) Representative H&E-stained section from the bladder of a mouse treated with a single dose of CPP. Scale bar, 50 μm.

(H) Expression of CD45 in sections from bladders of mice treated with a single dose of CPP. Scale bar, 50 μm.

(I) A section from a *Upk2CreERT2mTmG* mouse showing lack of Gfp-labeling in binucleated I cells after five cycles of CPP-induced injury and repair (purple arrows). Inset is Upk staining alone in a lower magnification image of the same section.

(legend continued on next page)

5N). CPP is used to treat leukemia, but is also a carcinogen that causes hemorrhagic cystitis (Cox, 1979; Farsund and Dahl, 1978; Golubeva et al., 2014). Whether serial injury plays a role in carcinogenesis by altering the behavior of urothelial cell types, is an interesting possibility.

DISCUSSION

The urothelium forms a barrier that prevents exchange of water and toxins between the urinary tract and the blood. S-cells, which are binucleated and polyploid, line the apical surface of the urothelium and perform many functions that are critical for maintaining the urothelial barrier (reviewed in Khandelwal et al. [2009]; Wu et al. [2009]). S-cells are long-lived, surviving 40 weeks or longer (Farsund, 1975). They are connected to one another via high-resistance tight junctions, and their apical surface is lined with Upk-containing plaque, features important for protecting against pathogens and toxins, for preventing leakage of urine into underlying tissue, and preventing water loss. S-cells maintain a system of fusiform vesicles that transport Upks from the Golgi to the cell surface where they assemble into plaque, and a second system of endosomal vesicles that transport apical membrane and plaque back into the cells for degradation (Amano et al., 1991; Khandelwal et al., 2009; Wu et al., 2009). Polyploidy and endomitosis may be critical in S-cells for a number of important functions. The ability to adjust DNA concentration without undergoing cell division may enable S-cells to respond to environmental changes without disrupting the urothelial barrier, and the presence of a binucleated I-cell population just below the Superficial layer, provides a population of progenitors that can quickly replace S-cells as they die off, thereby maintaining the urothelial barrier.

S-Cells Form from Binucleated I-Cells and S-Cells via Endomitosis and Endoreplication

Polyploid cells are common in the plant kingdom and are increasingly found in cells and tissues in the animal kingdom. In *Drosophila*, they include nurse cells, salivary gland cells, ovarian follicle cells, and glia cells (Frawley and Orr-Weaver, 2015; Hammond and Laird, 1985; Unhavaithaya and Orr-Weaver, 2012); in zebrafish, they include epicardium (Cao et al., 2017); and in mammals, they include hepatocytes (Duncan, 2013; Fortier et al., 2017), megakaryocytes (Machlus and Italiano, 2013), and syncytial trophoblasts (Hu and Cross, 2010), among others. They generally arise via successive rounds of cell fusion; via endomitosis, in which cells progress through mitosis but fail to complete cell division, resulting in binucleation; or via endoreplication or endocycling in which cells completely bypass mitosis and instead alternate between G and S phases (Lee et al., 2009; Orr-Weaver, 2015).

To visualize urothelial cell division in real time, we developed an organotypic culture system, in which we culture thick sections of urothelium and associated stroma. Our system maintains the stratification and cell types present in the *in vivo* urothelium for up to 1 month. We developed a mouse strain (*Upk2CreERT2; mTmG;nTnG* mice) expressing both membrane-bound *Gfp* and nuclear *Gfp* in I- and S-cells, enabling us to simultaneously visualizate of nuclei and cell boundaries during cell division. Real-time imaging of *Upk2CreERT2;mTmG;nTnG* cultures revealed mononucleated I-cells in the process of cytokinesis, undergoing normal cell division, and mononucleated I-cells entering mitosis without undergoing cytokinesis, a process known as endomitosis. In this case, binucleated cells progress to anaphase and develop a contractile ring and cytokinetic furrow that subsequently regresses, generating a binucleated cell with two diploid ($2n$+$2n$) nuclei.

S-cells are post-mitotic and have a DNA content of 8n ($4n$+$4n$), twice that of I-cells. Importantly, we have not observed either binucleated I- or S-cells at any stage of mitosis, indicating that this further increase in ploidy is unlikely to occur during cell division. Pulse labeling with EdU during regeneration indicates that binucleated I-cells, which initially have a DNA content of $4n$ (2n+2n), can enter S phase as they differentiate into newly formed S-cells. Interestingly, these experiments suggest that S-cells can also enter S phase, perhaps enabling them to directly respond to environmental or metabolic changes. The ability of S-cells to endocycle, as opposed to undergo cell division, may also help maintain urothelial impermeability, which depends on high-resistance tight junctions that prevent leakage during micturition (Rickard et al., 2008)

While the function of polyploidy remains unclear, a number of studies suggest that the large amount of DNA and the ability to adjust DNA content without entering mitosis may enable terminally differentiated cells to respond more efficiently to environmental changes (Bergmann et al., 2015; Duncan, 2013; Guidotti et al., 2003; Losick et al., 2013; Pandit et al., 2013). Polyploidy is associated with increased cell size in plants, insects, and animals (Beaulieu et al., 2008; Epstein, 1967; Orr-Weaver, 2015), and polyploid cells are susceptible to aneuploidy and can lead to cancer, since they evade the regular cell cycle checkpoints that would normally induce apoptosis (Gordon et al., 2012). On the other hand, recent studies suggest that polyploid hepatocytes suppress tumorigenesis compared to diploid hepatocytes (Zhang et al., 2018). The urothelium is a source of cells that produce bladder cancers. The extremely slow rate of urothelial turnover (almost 1 year) may be a factor that helps prevent aneuploidy and tumorigenesis. Whether polyploidy in the binucleated I-cell or S-cell populations leads to increased or reduced tendency for bladder cancer is an interesting question.

Binucleated S-Cells Are Generated via Similar Pathways Whether They Arise from I-Cells or Basal Cells

Lineage studies in mice aimed at defining S-cell progenitors during urothelial regeneration yield conflicting results. In some cases, basal cells have been identified as progenitors, but, in

(J) A section from a *Upk2CreERT2mTmG* mouse after 5X CPP treatment. Yellow arrows point to b inucleated S-cells, which are unlabeled.
(K) A section from *Krt5CreERT2mTmG* mouse showing Gfp-labeled binucleated I-cells (purple arrows) after five cycles of CPP-induced regeneration and repair.
(L) A section from *Krt5CreERT2mTmG* mouse showing Gfp-labeled binucleated S-cells (yellow arrows) after five cycles of CPP-induced regeneration and repair.
(M) Representative H&E-stained section of a bladder from a mouse treated with five doses of CPP. Scale bar, 50 μm.
(N) Expression of CD45 in sections from a mouse treated with five doses of CPP. Scale bar, 50 μm.

others, I-cells have been identified as progenitors (Colopy et al., 2014; Gandhi et al., 2013; Mysorekar et al., 2009; reviewed in Balsara and Li [2017]; Paraskevopoulou et al. [2016]; Wang et al. [2017]; Yamany et al. [2014]). A potential explanation for these disparities comes from recent fate mapping studies comparing the potential of I-cells and basal cells in a surgical model of bladder augmentation (Schäfer et al., 2017). This analysis indicates that both I and basal cells contribute to urothelial repair in response to focal injury, whereas basal cells alone were able to produce urothelial cells *de novo*, suggesting that differences in the extent or type of injury affect the regenerative potential of I-cells and basal cells (Schäfer et al., 2017). Our results agree with these observations. Using two different models, we show that mononucleated I-cells can produce S-cells in response to acute injury, with a smaller contribution from basal cells, but, after serial injury, I-cells are depleted and basal cells give rise to I- and S-cells, a feature that is likely to be critical for maintaining the urothelial barrier. Whether basal cell lineage capacity or I-cells depletion in chronic or repeated injury are a response to factors secreted from immune cells, is an interesting question. Recurrent UTI, chronic injury, and indwelling catheters can damage the urothelium, leading to abnormal differentiation and disease. Thus, defining the molecular pathways that are altered in the urothelium by chronic injury and inflammation will be important for developing new strategies to promote urothelial regeneration and repair.

STAR★METHODS

Detailed methods are provided in the online version of this paper and include the following:

- KEY RESOURCES TABLE
- CONTACT FOR REAGENT AND RESOURCE SHARING
- EXPERIMENTAL MODEL AND SUBJECT DETAILS
  - *In Vitro* Studies Organotypic culture and time lapse recording
  - *In Vivo* Animal Studies Mice
  - UTI with Uropathogenic
  - Bacterial strain UTI
  - Chemical Injury
  - Pulse-Chase experiments
- METHOD DETAILS
  - Genotyping
  - Tamoxifen and 4-OHT administration
  - Immunostaining
  - Microscopy
- QUANTIFICATION AND STATISTICAL ANALYSIS
  - DNA content analysis
  - Statistical Analysis

SUPPLEMENTAL INFORMATION

Supplemental Information includes three figures and two videos and can be found with this article online at https://doi.org/10.1016/j.celrep.2018.09.042.

ACKNOWLEDGMENTS

We thank Daniel Metzger and Pierre Chambon for the *K5CreERT2* line, Ben Ohlstein for discussions and comments, Carlos Cordon-Cardo for the *Up2CreERT2* line, and Andy McMahon for the *Upk3aGCE* line. We thank the Scott Hultgren lab for the gift of UTI strain 89 and Henry Sun and Xue-Rue Wu for antibodies and helpful discussions. Confocal and multiphoton images were collected and analyzed in the Confocal and Specialized Microscopy Shared Resource of the Herbert Irving Comprehensive Cancer Center at Columbia University, which is supported by an NIH grant (P30 CA013696) (National Cancer Institute). This work was supported by NIH grants (R01 DK95044 to C.L.M.; R01GM117407 to J.C.C.; and R01 DK100644 to I.U.M.).

AUTHOR CONTRIBUTIONS

J.W. performed most of the immunostaining analysis. J.W., S.S., T.T., and C.L. analyzed the DNA content. J.W., G.W., H.D., and C.D.L. performed the CPP experiments and analyzed the CPP data. E.B. developed the organotypic culture, and T.S. helped with acquisition/processing of real-time images. K.S. and S.S. performed UTI experiments. G.W. and J.W. performed the pulse-chase experiments. Y.Z., K.S., J.W., and C.L.M. quantified data from experiments and performed statistical analysis. Y.Z., J.C.C., and C.M. generated figures. C.L.M., Y.Z., and J.W. wrote the manuscript and assembled the figures. I.U.M., J.C.C., Y.Z., and C.L.M. worked on revisions and responses to reviewer comments. C.L.M. supervised the experiments and organized the study.

DECLARATION OF INTERESTS

The authors declare no competing interests.

Received: February 15, 2018
Revised: May 28, 2018
Accepted: September 12, 2018
Published: October 9, 2018

REFERENCES

Amano, O., Kataoka, S., and Yamamoto, T.Y. (1991). Turnover of asymmetric unit membranes in the transitional epithelial superficial cells of the rat urinary bladder. Anat. Rec. *229*, 9–15.

Balsara, Z.R., and Li, X. (2017). Sleeping beauty: awakening urothelium from its slumber. Am. J. Physiol. Renal Physiol. *312*, F732–F743.

Batourina, E., Gandhi, D., Mendelsohn, C.L., and Molotkov, A. (2012). Organotypic culture of the urogenital tract. Methods Mol. Biol. *886*, 45–53.

Beaulieu, J.M., Leitch, I.J., Patel, S., Pendharkar, A., and Knight, C.A. (2008). Genome size is a strong predictor of cell size and stomatal density in angiosperms. New Phytol. *179*, 975–986.

Bergmann, O., Zdunek, S., Felker, A., Salehpour, M., Alkass, K., Bernard, S., Sjostrom, S.L., Szewczykowska, M., Jackowska, T., Dos Remedios, C., et al. (2015). Dynamics of cell generation and turnover in the human heart. Cell *161*, 1566–1575.

Caldas, H., Jiang, Y., Holloway, M.P., Fangusaro, J., Mahotka, C., Conway, E.M., and Altura, R.A. (2005). Survivin splice variants regulate the balance between proliferation and cell death. Oncogene *24*, 1994–2007.

Cao, J., Wang, J., Jackman, C.P., Cox, A.H., Trembley, M.A., Balowski, J.J., Cox, B.D., De Simone, A., Dickson, A.L., Di Talia, S., et al. (2017). Tension creates an endoreplication wavefront that leads regeneration of epicardial tissue. Dev. Cell *42*, 600–615.e4.

Carattino, M.D., Prakasam, H.S., Ruiz, W.G., Clayton, D.R., McGuire, M., Gallo, L.I., and Apodaca, G. (2013). Bladder filling and voiding affect umbrella cell tight junction organization and function. Am. J. Physiol. Renal Physiol. *305*, F1158–F1168.

Carmena, M., and Earnshaw, W.C. (2003). The cellular geography of aurora kinases. Nat. Rev. Mol. Cell Biol. *4*, 842–854.

Chen, S.L., Hung, C.S., Xu, J., Reigstad, C.S., Magrini, V., Sabo, A., Blasiar, D., Bieri, T., Meyer, R.R., Ozersky, P., et al. (2006). Identification of genes subject to positive selection in uropathogenic strains of Escherichia coli: a comparative genomics approach. Proc. Natl. Acad. Sci. USA *103*, 5977–5982.

Colopy, S.A., Bjorling, D.E., Mulligan, W.A., and Bushman, W. (2014). A population of progenitor cells in the basal and intermediate layers of the murine bladder urothelium contributes to urothelial development and regeneration. Dev. Dyn. *243*, 988–998.

Cox, P.J. (1979). Cyclophosphamide cystitis–identification of acrolein as the causative agent. Biochem. Pharmacol. *28*, 2045–2049.

DePamphilis, M.L. (2016). Genome duplication: the heartbeat of developing organisms. Curr. Top. Dev. Biol. *116*, 201–229.

Duncan, A.W. (2013). Aneuploidy, polyploidy and ploidy reversal in the liver. Semin. Cell Dev. Biol. *24*, 347–356.

Duncan, A.W., Taylor, M.H., Hickey, R.D., Hanlon Newell, A.E., Lenzi, M.L., Olson, S.B., Finegold, M.J., and Grompe, M. (2010). The ploidy conveyor of mature hepatocytes as a source of genetic variation. Nature *467*, 707–710.

Edgar, B.A., and Orr-Weaver, T.L. (2001). Endoreplication cell cycles: more for less. Cell *105*, 297–306.

Edgar, B.A., Zielke, N., and Gutierrez, C. (2014). Endocycles: a recurrent evolutionary innovation for post-mitotic cell growth. Nat. Rev. Mol. Cell Biol. *15*, 197–210.

Epstein, C.J. (1967). Cell size, nuclear content, and the development of polyploidy in the Mammalian liver. Proc. Natl. Acad. Sci. USA *57*, 327–334.

Farsund, T. (1975). Cell kinetics of mouse urinary bladder epithelium. I. Circadian and age variations in cell proliferation and nuclear DNA content. Virchows Arch. B Cell Pathol. Incl. Mol. Pathol. *18*, 35–49.

Farsund, T., and Dahl, E. (1978). Cell kinetics of mouse urinary bladder epithelium. III. A histologic and ultrastructural study of bladder epithelium during regeneration after a single dose of cyclophosphamide, with special reference to the mechanism by which polyploid cells are formed. Virchows Arch. B Cell Pathol. Incl. Mol. Pathol. *26*, 215–223.

Field, C.M., and Alberts, B.M. (1995). Anillin, a contractile ring protein that cycles from the nucleus to the cell cortex. J. Cell Biol. *131*, 165–178.

Fortier, M., Celton-Morizur, S., and Desdouets, C. (2017). Incomplete cytokinesis/binucleation in mammals: The powerful system of hepatocytes. Methods Cell Biol. *137*, 119–142.

Fox, D.T., and Duronio, R.J. (2013). Endoreplication and polyploidy: insights into development and disease. Development *140*, 3–12.

Frawley, L.E., and Orr-Weaver, T.L. (2015). Polyploidy. Curr. Biol. *25*, R353–R358.

Gandhi, D., Molotkov, A., Batourina, E., Schneider, K., Dan, H., Reiley, M., Laufer, E., Metzger, D., Liang, F., Liao, Y., et al. (2013). Retinoid signaling in progenitors controls specification and regeneration of the urothelium. Dev. Cell *26*, 469–482.

Garofalo, C.K., Hooton, T.M., Martin, S.M., Stamm, W.E., Palermo, J.J., Gordon, J.I., and Hultgren, S.J. (2007). Escherichia coli from urine of female patients with urinary tract infections is competent for intracellular bacterial community formation. Infect. Immun. *75*, 52–60.

Gentric, G., and Desdouets, C. (2014). Polyploidization in liver tissue. Am. J. Pathol. *184*, 322–331.

Golubeva, A.V., Zhdanov, A.V., Mallel, G., Dinan, T.G., and Cryan, J.F. (2014). The mouse cyclophosphamide model of bladder pain syndrome: tissue characterization, immune profiling, and relationship to metabotropic glutamate receptors. Physiol. Rep. *2*, e00260.

Gordon, D.J., Resio, B., and Pellman, D. (2012). Causes and consequences of aneuploidy in cancer. Nat. Rev. Genet. *13*, 189–203.

Guidotti, J.E., Brégerie, O., Robert, A., Debey, P., Brechot, C., and Desdouets, C. (2003). Liver cell polyploidization: a pivotal role for binuclear hepatocytes. J. Biol. Chem. *278*, 19095–19101.

Hammond, M.P., and Laird, C.D. (1985). Chromosome structure and DNA replication in nurse and follicle cells of Drosophila melanogaster. Chromosoma *91*, 267–278.

Harfe, B.D., Scherz, P.J., Nissim, S., Tian, H., McMahon, A.P., and Tabin, C.J. (2004). Evidence for an expansion-based temporal Shh gradient in specifying vertebrate digit identities. Cell *118*, 517–528.

Hicks, R.M. (1975). The mammalian urinary bladder: an accommodating organ. Biol. Rev. Camb. Philos. Soc. *50*, 215–246.

Hu, D., and Cross, J.C. (2010). Development and function of trophoblast giant cells in the rodent placenta. Int. J. Dev. Biol. *54*, 341–354.

Hung, C.S., Dodson, K.W., and Hultgren, S.J. (2009). A murine model of urinary tract infection. Nat. Protoc. *4*, 1230–1243.

Indra, A.K., Warot, X., Brocard, J., Bornert, J.M., Xiao, J.H., Chambon, P., and Metzger, D. (1999). Temporally-controlled site-specific mutagenesis in the basal layer of the epidermis: comparison of the recombinase activity of the tamoxifen-inducible Cre-ER(T) and Cre-ER(T2) recombinases. Nucleic Acids Res. *27*, 4324–4327.

Jost, S.P. (1986). Renewal of normal urothelium in adult mice. Virchows Arch. B Cell Pathol. Incl. Mol. Pathol. *51*, 65–70.

Jost, S.P., and Potten, C.S. (1986). Urothelial proliferation in growing mice. Cell Tissue Kinet. *19*, 155–160.

Khandelwal, P., Abraham, S.N., and Apodaca, G. (2009). Cell biology and physiology of the uroepithelium. Am. J. Physiol. Renal Physiol. *297*, F1477–F1501.

Le Bras, S., and Le Borgne, R. (2014). Epithelial cell division - multiplying without losing touch. J. Cell Sci. *127*, 5127–5137.

Lee, H.O., Davidson, J.M., and Duronio, R.J. (2009). Endoreplication: polyploidy with purpose. Genes Dev. *23*, 2461–2477.

Lin, J.H., Wu, X.R., Kreibich, G., and Sun, T.T. (1994). Precursor sequence, processing, and urothelium-specific expression of a major 15-kDa protein subunit of asymmetric unit membrane. J. Biol. Chem. *269*, 1775–1784.

Losick, V.P., Fox, D.T., and Spradling, A.C. (2013). Polyploidization and cell fusion contribute to wound healing in the adult Drosophila epithelium. Curr. Biol. *23*, 2224–2232.

Machlus, K.R., and Italiano, J.E., Jr. (2013). The incredible journey: From megakaryocyte development to platelet formation. J. Cell Biol. *201*, 785–796.

Muzumdar, M.D., Tasic, B., Miyamichi, K., Li, L., and Luo, L. (2007). A global double-fluorescent Cre reporter mouse. Genesis *45*, 593–605.

Mysorekar, I.U., Isaacson-Schmid, M., Walker, J.N., Mills, J.C., and Hultgren, S.J. (2009). Bone morphogenetic protein 4 signaling regulates epithelial renewal in the urinary tract in response to uropathogenic infection. Cell Host Microbe *5*, 463–475.

Nguyen, H.G., and Ravid, K. (2010). Polyploidy: mechanisms and cancer promotion in hematopoietic and other cells. Adv. Exp. Med. Biol. *676*, 105–122.

Oliferenko, S., Chew, T.G., and Balasubramanian, M.K. (2009). Positioning cytokinesis. Genes Dev. *23*, 660–674.

Orr-Weaver, T.L. (2015). When bigger is better: the role of polyploidy in organogenesis. Trends Genet. *31*, 307–315.

Pandit, S.K., Westendorp, B., and de Bruin, A. (2013). Physiological significance of polyploidization in mammalian cells. Trends Cell Biol. *23*, 556–566.

Papafotiou, G., Paraskevopoulou, V., Vasilaki, E., Kanaki, Z., Paschalidis, N., and Klinakis, A. (2016). KRT14 marks a subpopulation of bladder basal cells with pivotal role in regeneration and tumorigenesis. Nat. Commun. *7*, 11914.

Paraskevopoulou, V., Papafotiou, G., and Klinakis, A. (2016). KRT14 marks bladder progenitors. Cell Cycle *15*, 3161–3162.

Prigge, J.R., Wiley, J.A., Talago, E.A., Young, E.M., Johns, L.L., Kundert, J.A., Sonsteng, K.M., Halford, W.P., Capecchi, M.R., and Schmidt, E.E. (2013). Nuclear double-fluorescent reporter for in vivo and ex vivo analyses of biological transitions in mouse nuclei. Mamm. Genome, Published online September 11, 2013. https://doi.org/10.1007/s00335-013-9469-8.

Rickard, A., Dorokhov, N., Ryerse, J., Klumpp, D.J., and McHowat, J. (2008). Characterization of tight junction proteins in cultured human urothelial cells. In Vitro Cell. Dev. Biol. Anim. *44*, 261–267.

Rios, A.C., Fu, N.Y., Jamieson, P.R., Pal, B., Whitehead, L., Nicholas, K.R., Lindeman, G.J., and Visvader, J.E. (2016). Essential role for a novel population of binucleated mammary epithelial cells in lactation. Nat. Commun *7*, 11400.

Sambandamoorthy, S., Mathew-Steiner, S., Varney, S., Zuidema, J.M., Gilbert, R.J., Van De Water, L., and LaFlamme, S.E. (2015). Matrix compliance and the regulation of cytokinesis. Biol. Open *4*, 885–892.

Sarto, G.E., Stubblefield, P.A., and Therman, E. (1982). Endomitosis in human trophoblast. Hum. Genet. *62*, 228–232.

Schäfer, F.M., Algarrahi, K., Savarino, A., Yang, X., Seager, C., Franck, D., Costa, K., Liu, S., Logvinenko, T., Adam, R., and Mauney, J.R. (2017). Mode of surgical injury influences the source of urothelial progenitors during bladder defect repair. Stem Cell Reports *9*, 2005–2017.

Schindelin, J., Arganda-Carreras, I., Frise, E., Kaynig, V., Longair, M., Pietzsch, T., Preibisch, S., Rueden, C., Saalfeld, S., Schmid, B., et al. (2012). Fiji: an open-source platform for biological-image analysis. Nat. Methods *9*, 676–682.

Schneider, C.A., Rasband, W.S., and Eliceiri, K.W. (2012). NIH Image to ImageJ: 25 years of image analysis. Nat. Methods *9*, 671–675.

Schoenfelder, K.P., and Fox, D.T. (2015). The expanding implications of polyploidy. J. Cell Biol. *209*, 485–491.

Shen, T.H., Gladoun, N., Castillo-Martin, M., Bonal, D., Domingo-Domenech, J., Charytonowicz, D., and Cordon-Cardo, C. (2012). A BAC-based transgenic mouse specifically expresses an inducible Cre in the urothelium. PLoS ONE *7*, e35243.

Shin, K., Lee, J., Guo, N., Kim, J., Lim, A., Qu, L., Mysorekar, I.U., and Beachy, P.A. (2011). Hedgehog/Wnt feedback supports regenerative proliferation of epithelial stem cells in bladder. Nature *472*, 110–114.

Stewart, F.A. (1986). Mechanism of bladder damage and repair after treatment with radiation and cytostatic drugs. Br. J. Cancer Suppl. *7*, 280–291.

Storchova, Z., and Pellman, D. (2004). From polyploidy to aneuploidy, genome instability and cancer. Nat. Rev. Mol. Cell Biol. *5*, 45–54.

Swanhart, L., Kupsco, J., and Duronio, R.J. (2005). Developmental control of growth and cell cycle progression in Drosophila. Methods Mol. Biol. *296*, 69–94.

Taniguchi, K., Kokuryo, A., Imano, T., Minami, R., Nakagoshi, H., and Adachi-Yamada, T. (2014). Isoform-specific functions of Mud/NuMA mediate binucleation of Drosophila male accessory gland cells. BMC Dev. Biol. *14*, 46.

Unhavaithaya, Y., and Orr-Weaver, T.L. (2012). Polyploidization of glia in neural development links tissue growth to blood-brain barrier integrity. Genes Dev. *26*, 31–36.

Van Batavia, J., Yamany, T., Molotkov, A., Dan, H., Mansukhani, M., Batourina, E., Schneider, K., Oyon, D., Dunlop, M., Wu, X.R., et al. (2014). Bladder cancers arise from distinct urothelial sub-populations. Nat. Cell Biol. *16*, 982–991.

Vasconcelos-Nóbrega, C., Colaço, A., Lopes, C., and Oliveira, P.A. (2012). Review: BBN as an urothelial carcinogen. In Vivo *26*, 727–739.

Wang, C., Ross, W.T., and Mysorekar, I.U. (2017). Urothelial generation and regeneration in development, injury, and cancer. Dev. Dyn. *246*, 336–343.

Wu, X.R., Manabe, M., Yu, J., and Sun, T.T. (1990). Large scale purification and immunolocalization of bovine uroplakins I, II, and III. Molecular markers of urothelial differentiation. J. Biol. Chem. *265*, 19170–19179.

Wu, X.R., Lin, J.H., Walz, T., Häner, M., Yu, J., Aebi, U., and Sun, T.T. (1994). Mammalian uroplakins. A group of highly conserved urothelial differentiation-related membrane proteins. J. Biol. Chem. *269*, 13716–13724.

Wu, X.R., Kong, X.P., Pellicer, A., Kreibich, G., and Sun, T.T. (2009). Uroplakins in urothelial biology, function, and disease. Kidney Int. *75*, 1153–1165.

Yamany, T., Van Batavia, J., and Mendelsohn, C. (2014). Formation and regeneration of the urothelium. Curr. Opin. Organ Transplant. *19*, 323–330.

Zhang, S., Zhou, K., Luo, X., Li, L., Tu, H.C., Sehgal, A., Nguyen, L.H., Zhang, Y., Gopal, P., Tarlow, B.D., et al. (2018). The polyploid state plays a tumor-suppressive role in the liver. Dev. Cell *44*, 447–459.e5.

STAR★METHODS

KEY RESOURCES TABLE

REAGENT or RESOURCE	SOURCE	IDENTIFIER
Antibodies		
p63 (4A4) antibody	Santa Cruz Biotechnology	sc8431; RRID:AB_628091
p63 antibody [N2C1], Internal	GenTex	GTX102425; RRID:AB_1952344
Keratin 5 Polyclonal Antibody	Covance	PRB-160P; RRID:AB_10063444
Keratin 5 Polyclonal Chicken Antibody	Covance	SIG-3475; RRID:AB_10720202
Cytokeratin 20 antibody	DAKO	M7019; RRID:AB_2133718
Ki67 antibody - Proliferation Marker	Abcam	ab15580; RRID:AB_443209
Green Fluorescent Protein (GFP) Antibody	AVES Lab	GFP-1020, RRID:AB_10000240
UPIII (M-17) antibody	Santa Cruz Biotechnology	sc-15186; RRIDAB_671435
Survivin (71G4B7) Rabbit mAb antibody	Cell signaling technology	2808S; RRID:AB_10691694
Mouse monoclonal Anti-beta-Tubulin antibody	Sigma	T4026; RRID:AB_477577
Phospho-Histone H3 (Ser10) (6G3) Mouse monoclonal Antibody	Cell signaling technology	9706S; RRID:AB_331748
Rabbit Anti-Cyclin D1 Monoclonal Antibody	Abcam	ab16663; RRID:AB_443423
Goat Anti-Mouse E-cadherin Polyclonal antibody, Unconjugated	R&D system	AF748; RRID:AB_355568
Anti-RFP (RABBIT) Polyclonal Antibody	Rockland	600-401-379; RRID:AB_2209751
Aurora A/B kinase, Mouse monoclonal	EnCor Biotechnology	MCA-5A12; RRID:AB_2572231
Anillin Antibody, Rabbit Polyclonal	Novus	NBP1-31060; RRID:AB_2058287
Alexa Fluor® 488-AffiniPure Donkey Anti-Rabbit IgG (H+L) antibody	Jackson Immuno-Research Labs	711-545-152; RRID:AB_2313584
Alexa Fluor 488-AffiniPure Donkey Anti-Mouse IgG (H+L) antibody	Jackson Immuno-Research Labs	715-545-150; RRID:AB_2340846
Cy3-AffiniPure Donkey Anti-Rabbit IgG (H+L) antibody	Jackson Immuno-Research Labs	711-165-152; RRID:AB_2307443
Alexa Fluor 594-AffiniPure Donkey Anti-Mouse IgG (H+L) antibody	Jackson Immuno-Research Labs	715-585-151; RRID:AB_2340855
Alexa Fluor 647-AffiniPure Donkey Anti-Mouse IgG (H+L) antibody	Jackson Immuno-Research Labs	715-605-150; RRID:AB_2340862
Alexa Fluor 647-AffiniPure Donkey Anti-Rabbit IgG (H+L) antibody	Jackson Immuno-Research Labs	711-605-152; RRID:AB_2492288
Alexa Fluor 488 AffiniPure Donkey Anti-Chicken IgY (IgG) (H+L) antibody	Jackson Immuno-Research Labs	703-545-155; RRID:AB_2340375
Alexa Fluor 594-AffiniPure Donkey Anti-Chicken IgY (IgG) (H+L) antibody	Jackson Immuno-Research Labs	703-585-155; RRID:AB_2340377
Bacterial and Virus Strains		
Uropathogenic *E.coli* Strain UTI 89	Gift from Scott Hultgren Lab	N/A
Biological Samples		
Mouse adult female bladder, UTI infected and control animals.	This paper	N/A
Mouse urothelium; dissected tissue for the organotypic culture.	This paper	N/A
Mouse urothelium, CPP-treated male/female.	This Paper	N/A
Chemicals, Peptides, and Recombinant Proteins		
EdU (5-ethynyl-2′-deoxyuridine), pulse chase	Invitrogen	Cat# A10044
Tamoxifen, for inducing Cre recombinase	Sigma	cat# T5648

(*Continued on next page*)

Continued

REAGENT or RESOURCE	SOURCE	IDENTIFIER
4-OHT, for urothelial culture	Sigma	#H7904
CPP for injury/repair model	Sigma	cat #C7397
KSFM and supplements for tissue culture	GIBCO	#17005042
Critical Commercial Assays		
Click-iT EdU Alexa Fluor 647 Imaging Kit	Invitrogen	Cat#C10340
Experimental Models: Organisms/Strains		
Mouse line; FVB.Cg–Tg(KRT5–cre/ERT2) 2Ipc/JeldJ	Obtained from D. Metzger and P. Chambon (Indra et al., 1999)	RRID:IMSR_JAX:018394
Mouse line; Upk2CreERT (B6;CBA-Tg (Upk2-icre/ERT2)1Ccc)	Obtained from the Cordon-Cardo lab. (Shen et al., 2012)	RRID:IMSR_JAX:024768
Mouse line Upk3aGCE (B6;DBA-Tg (Upk3a-GFP/cre/ERT2)26Amc/J	Obtained from the McMahon lab	RRID:IMSR_JAX:015855
Mouse line B6;129S6-Gt(ROSA) 26Sor$^{tm14(CAG-tdTomato)Hze}$/J, (Rosa26;mCherry)	The Jackson Laboratory	RRID:IMSR_JAX:007908
Mouse line Rosa26mTmG *B6.129(Cg) Gt(ROSA)26Sortm4$^{(ACTB–\ tdTomato,–EGFP)\ Luo/J33)}$	The Jackson Laboratory (Muzumdar et al., 2007)	RRID:IMSR_JAX:007676
Oligonucleotides		
Forward Upk2CreER: CATTGCCCCTGTTTCACTATC	This paper	N/A
Reverse Upk2CreER CAATGATGTTTCACTGGTTATG	This paper	N/A
Forward Krt5CreER ATTTGCCTGCATTACCGGTC	This paper	N/A
Reverse Krt5CreER ATCAACGTTTTGTTTTCGGA	This paper	N/A
Forward R26mGmT/R26nTnG CTCTGCTGCCTC CTGGCTTCT	This paper	N/A
Reverse R26mGmT/R26nTnG TCAATGGGCGG GGGTCGTT	This paper	N/A
Forward Upk3aGCE AGGAGCTTTGCAGAAGACCA	This paper	N/A
Reverse Upk3aGCE GAACTTCAGGGTCAGCTTGC	This paper	N/A
Forward Rosa26;mCherry GGCATTAAAGCAGC GTATCC	This paper	N/A
Reverse Rosa26;mCherry CTGTTCCTGTACGG CATGG	This paper	N/A
Software and Algorithms		
NIS-Elements	Nikon	RRID:SCR_014329; https://www.nikon.com/products/microscope-solutions/support/download/software/imgsfw/nis_v41100mac.htm
Fiji package ImageJ	ImageJ	https://fiji.sc/
Prism	GraphPad	PRISM, RRID:SCR_005375 RRID:SCR_000306; https://www.graphpad.com/scientific-software/prism/
Other		
Zeiss Axiovert 200M microscope with an Apotome	Zeiss	N/A
Nikon Eclipse TE200 microscope	Nikon	N/A
Confocal microscopy, A1R MP confocal microscope	Nikon	N/A

CONTACT FOR REAGENT AND RESOURCE SHARING

Requests for reagents or resources should be directed to the Lead Contact, Cathy Mendelsohn (clm20@cumc.columbia.edu).

EXPERIMENTAL MODEL AND SUBJECT DETAILS

In Vitro Studies Organotypic culture and time lapse recording

Bladder tissue (urothelium and associated stroma) was isolated from male and female *UPCreER;mTmG/UPCreER,nTnG* mice and dissected into small pieces, approximately 0.3 to 0.5 cm in size, then cultured in KFSM medium with 10%FBS, EGF 5ng/ml, BPE 50ng/ml (supplements and KSFM, GIBCO #17005042 on collagen coated Millicell 0.4um 30mm filters, (Millipore) in glass-bottom microwell dishes (Mat-Tek Corporation, Ashland, MA, P35GCOL-0-14-C). 4-OHT was added to culture medium to induce Cre-dependent recombination, then tissue was incubated for an additional 24h, medium was replaced, and cultures were transferred to a stage-top incubator maintaining 37°C and 5% CO_2 (Tokai Hit, Shizuoka-ken, Japan) on a confocal microscope (A1R MP, Nikon Instruments, Melville, NY). Time-lapse multiphoton confocal images were captured using a 25x/1.1 Apochromat water-immersion objective. Excitation was at 920 nm, and emission was collected through standard GFP and RFP filters using a non-descanned detector. Time-lapse images were collected from 1-3 positions in the tissue every 4-6 min for 24hr. Z series were collected at each time point with a z interval of 3-4 0.3-0.4 μm Z sections and total stack size up to 50 μm.

In Vivo Animal Studies Mice

K5CreERT2 mice (*FVB.Cg–Tg(KRT5–cre/ERT2)2Ipc/JeldJ)32* were obtained from D. Metzger and P. Chambon at the IGBMC, France (Indra et al., 1999). This line was used in lineage tracing experiments in conjunction with Rosa26mTmG reporter mice *Gt(ROSA)26Sortm4*$^{(ACTB–\ tdTomato,–EGFP)\ Luo/J33}$. Controls for UTI and CPP experiments were uninfected/untreated Krt5CreERT2;Rosa26mTmG littermates, and Rosa26mTmG littermates lacking the Cre-recombinase. *Upk2CreERT2* mice (TgUICBAC mice) were generated in the Cordon-Cardo lab (Shen et al., 2012). This line was used in lineage/regenerative studies with the UTI and CPP models, and in organotypic culture with the *B6;129S6-Gt(ROSA)26Sor*$^{tm1(CAG-tdTomato*,-EGFP*)Ees}$/J reporter line (*Rosa26;nTnG* mice; Prigge et al., 2013). *Upk3aGCE* mice (Tg(Upk3a-GFP/cre/ERT2)26Amc) were from obtained from the McMahon lab, and are available from Jackson Labs. This line was used in conjunction with the mCherry line (B6;129S6-Gt(ROSA)26Sor$^{tm14(CAG-tdTomato)Hze}$/J), in lineage tracing experiments with the UTI model. Controls were uninfected Upk3aGCE females, and littermates (Upk3a-GFP/cre) without the tdTomato reporter strain. All experiments were carried out in triplicate (n = 3 experimental and control animals). All work with mice was approved by and performed under the regulations of the Columbia University Institutional Animal Care and Use Committee. Animals were housed in the animal facility of Irving Cancer Research Center, Columbia University. Protocol numbers and title: IUCUC #AC-AAAT7487. Lineage analysis of the urothelium; IUCUC #AC-AAAR0419: Analysis of the regenerative response of the urothelium. Bacterial suspensions were administered via transurethral catheter, hence UTI experiments were performed only on females. In all other experiments, females and male littermates or age matched animals were used for the experimental and controls in groups of n = 3 or more.

UTI with Uropathogenic

E. coli: Adult female mice (8-14 weeks) were anesthetized with isoflurane, and inoculated via transurethral catheterization with 75μl of bacterial suspension (10^7 cfu/ml) in phosphate-buffered saline (PBS) or 75ul sterile PBS according to the published protocol from the Hultgren Lab (Hung et al., 2009). EdU was administered to animals 24h after infection (0.1mg/20 g body weight) to label cells in S-phase. Urine was collected 4-6h p.i. assayed for bacterial counts and analyzed using the Cytospin and Hema3 staining Kit (Fisher Scientific). Titers of 10^6-10^7 CFU/ml were considered to be a robust infection. Sulfatrim (240mg/kg) was administered 30h after inoculation with UTI 89 to avoid reinfection. At the indicated times, mice were sacrificed, their bladders were aseptically removed and processed for microscopy and histology. Experiments were performed on females, due to anatomical constraints, and analysis was performed on n = 3 or greater bladder sample for each time-point/condition.

Bacterial strain UTI

E. coli UTI 89 was obtained from the Scott Hultgren lab (Chen et al., 2006). This strain was isolated from a patient with acute bladder infection (Chen et al., 2006). Cultures were prepared from freshly plated bacterial colonies.

Chemical Injury

For chemical injury, CPP (Sigma-Aldrich; catalog #C7397) was dissolved in PBS (15 mg/ml) and given to adult mice at a dose of 150 mg/kg by IP injection. In the case of chronic injury, CPP was administered 5X, with 2 weeks between each round of injury and repair, and bladders were analyzed 2 weeks after the last injection. Each group of animals included males and females, and analysis was performed on at least n = 3 control and experimental animals for each time point or condition. All work with mice was approved by and performed under the regulations of the Columbia University Institutional Animal Care and Use Committee. Animals were housed in the SPF animal facility of Irving Cancer Research Center, Columbia University. Protocol numbers and titles: IUCUC # AC-AAAT7487. Lineage analysis of the urothelium; IUCUC #AC-AAAR0419: Analysis of the regenerative response of the urothelium.

Pulse-Chase experiments

EdU was administered to animals during infection or after CPP injection (0.1mg/20 g body weight) to label cells in S-phase, animals were sacrificed 1h later, and analyzed to assess the distribution of Edu in the urothelium. All experiments were performed in triplicate.

METHOD DETAILS

Genotyping

Genotyping was done by PCR analysis of tail DNA. Primers for genotyping Upk2CreERT2 mice were 5′-CATTGCCCCTGTTTCAC TATC-3′ (forward) and 5′-CAATGATGTTTCACTGGTTATG-3′ (reverse), generating a 600 bp product. Primers for Krt5CreERT mice were 5′-ATTTGCCTGCATTACCGGTC-3′ (forward) and 5′-ATCAACGTTTTGTTTTCGGA-3′ (reverse), generating a 350 bp product. Primers for genotyping the R26mGmT and R26nTnG reporters were 5′-CTCTGC TGCCTCCTGGCTTCT-3′ (forward) and 5′-TCA ATGGGCGGGGGTCGTT-3′ (reverse), generating a 250 bp product. Primers for genotyping Upk3aGCE mice were: 5′-AGG AGCTTTGCAGAAGACCA (forward) and 5′-GAACTTCAGGGTCAGCTTGC (reverse), generating a 371 bp product. Primers for genotyping mCherry were: 5′-GGCATTAAAGCAGCGTATCC (forward) and CTGTTCCTGTACGGCATGG (reverse), generating a 196 bp product.

Tamoxifen and 4-OHT administration

Male and female adult mice (3 months of age) were injected with tamoxifen Sigma, cat# T5648, intraperitoneally, (5 mg per 30 g body weight) three times over a period of 7 days. For inducing Cre-dependent recombination in bladder explant cultures, 4-OHT (Sigma #H7904) was added to culture medium at a concentration of 200nM.

Immunostaining

Bladders were embedded in paraffin and serial sections were generated. For immunohistochemistry, sections were deparaffinized using HistoClear and rehydrated through a series of ethanol and 1XPBS washes. Antigen retrieval was performed by boiling slides for 30 min in buffer. Primary antibodies in 1% horse serum were incubated overnight at 4◦C. The next day, slides were washed with TBST 3 times for 10 min each and secondary antibodies were applied for 2h at room temperature. The following primary antibodies and concentrations were used in these studies: p63 mouse IgG (clone 4A4, Santa Cruz Biotechnology, sc8431, 1:100) or rabbit IgG, (GenTex, GTX102425, 1:300). CK5 rabbit IgG (Covance, AF-138, PRB- 160P, 1:300) or chicken IgY (Covance, SIG-3475, 1:300). CK20 antibody was mouse IgG2a, Kappa, clone Ks20.8 (DAKO, M7019, 1:250). Ki67 staining was with rabbit IgG (Abcam, ab15580, 1:300), GFP chicken IgY (AVES, GFP-1020, 1:300). UPK3a goat (Santa Cruz, 1:300), Survivin, rabbit IgG (Cell signaling, 2808S, 1:300), b-tubulin mouse (Sigma, T4026, 1:300), P-H3 (S-10), mouse (Cell signaling, 9706S, 1:200), Cyclin D1 rabbit (Abcam, ab16663, 1:300), E-cad goat (R&D system, AF748, 1:300), RFP rabbit (Rockland, #600-401-379,1:1000). Aurora A/B mouse (Encore, MCA-5A12, 1:200), Anillin (anti-rabbit; Novus, NBP1-31060, 1:300). The following secondary antibodies and concentrations were used in our studies: Jackson ImmunoResearch Alexa Fluor 488 donkey anti-rabbit IgG (711-545-152; 1:600), Alexa Fluor 488 donkey anti- mouse (715-545-150;1:600), CY3-conjugated donkey anti-rabbit IgG (711-165-152; 1:600), Alexa Fluor 594 donkey anti-mouse IgG (715-585-151; 1:500), Alexa Fluor 647-conjugated donkey anti-mouse IgG (715-605-150; 1:300), Alexa Fluor 647-conjugated donkey anti-rabbit IgG (711-605-152; 1:300), Alexa Fluor 488 donkey anti-chicken (703-545-155, 1:500), Alexa Fluor 594 donkey anti-chicken (703-585-155, 1:500). DAPI was either applied as part of the secondary antibodies cocktail or for 10 min, for nuclear staining, and then the slides were sealed with coverslips. Controls for antibody staining were either without primary antibody (negative control) or using tissue where the protein is known to be expressed (positive controls).

Microscopy

Immuno-fluorescence images were collected using a Zeiss Axiovert 200M microscope with an Apotome (Zeiss). Bright-field images were collected using a Nikon Eclipse TE200 microscope. Confocal microscopy was performed on an A1R MP confocal microscope (Nikon Instruments) and data was analyzed and rendered using NIS Elements (Nikon) and the Fiji package of ImageJ.

QUANTIFICATION AND STATISTICAL ANALYSIS

DNA content analysis

Stacks of images were obtained using confocal microscopy with 0.02 mm steps and 3D reconstructions were analyzed with the Fiji distribution of ImageJ (Schindelin et al., 2012; Schneider et al., 2012). Nuclei were segmented and incomplete nuclei were disregarded. The integrated density and volume of each nucleus were calculated. The ploidy of cells was determined by quantifying the intensity of DAPI within the nucleus. The average DAPI intensity of Basal cells was set as 2*n*. As shown in Figure S1, a total of 183 cells from three adult mice were quantified using Basal cells as a reference. Based on these measurements, mononuclear I-cells are assigned a ploidy of 2*n,* binucleated I-cells 4*n* (2*n*+2*n*), and S-cells 8*n* or larger (4*n*+4*n*).

Statistical Analysis

All quantification was performed on at least three independent biological samples, using the ImageJ software. Data presented are mean values ± s.e.m. Statistical analysis was performed using the GraphPad Prism software v6. In two group comparisons, statistical significance was determined using a two-tailed Student's t test, considering a value of $p < 0.05$ as significant. Multiple comparisons were performed using the Kruskal–Wallis statistical test. All sample sizes met the minimum requirements of the respective statistical test used.

Cell Reports, Volume *25*

Supplemental Information

Polyploid Superficial Cells that Maintain the Urothelial Barrier Are Produced via Incomplete Cytokinesis and Endoreplication

Jia Wang, Ekatherina Batourina, Kerry Schneider, Spenser Souza, Theresa Swayne, Chang Liu, Christopher D. George, Tiffany Tate, Hanbin Dan, Gregory Wiessner, Yelena Zhuravlev, Julie C. Canman, Indira U. Mysorekar, and Cathy Lee Mendelsohn

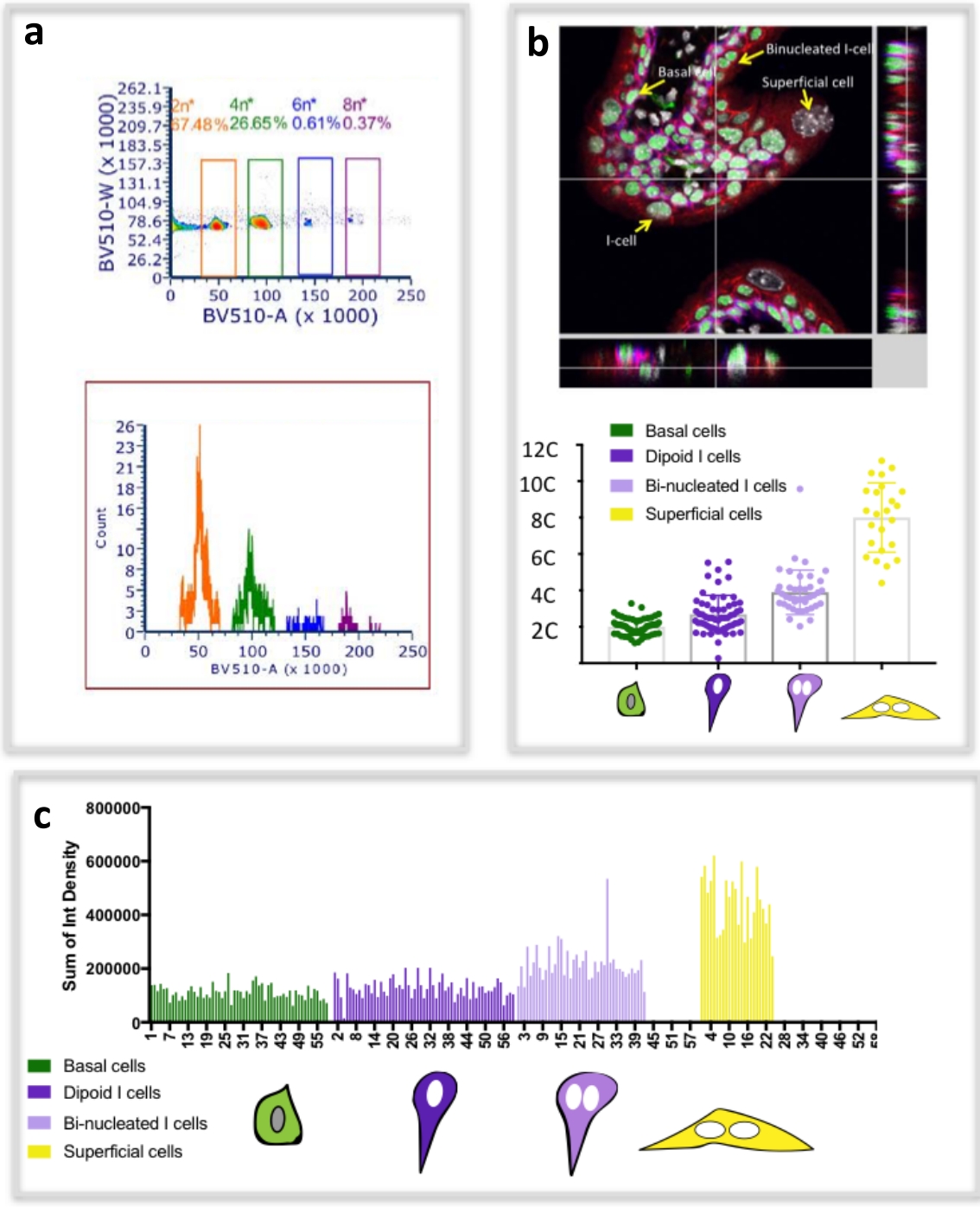

Figure S1. DNA content measurements, related to Figure 1.

(a) Relative DNA content obtained by flow cytometric analysis of propidium iodide-stained nuclei from the adult mouse urothelium. Basal cells which are 2*n*, served as internal reference standard. **(b)** A section of a urothelium from a UPEC infected mouse 25h post-infection stained for EdU and P63. EdU was administered 24h after infection and tissue was collected one hour later. The Dot Plot shows the estimated DNA content of urothelial sub-populations based on integrated fluorescence density of DAPI staining. For this experiment, we analyzed 59 basal cells, 58 mononucleated cells, 42 bi-nucleated I-cells and 24 S-cells. **(c)** The estimated DNA content of EdU+ cells was assessed by analysis of the Integrated Fluorescence density of DAPI stained sections The graph below shows the Sum of Estimated Density from analysis of EdU+ Basal cells, mononucleated I-cells, binucleated I-cells and S-cells at 25h and 72h post infection. For quantification, a minimum of three independent experiments were performed, and numbers are mean of percentages ± s.e.m.

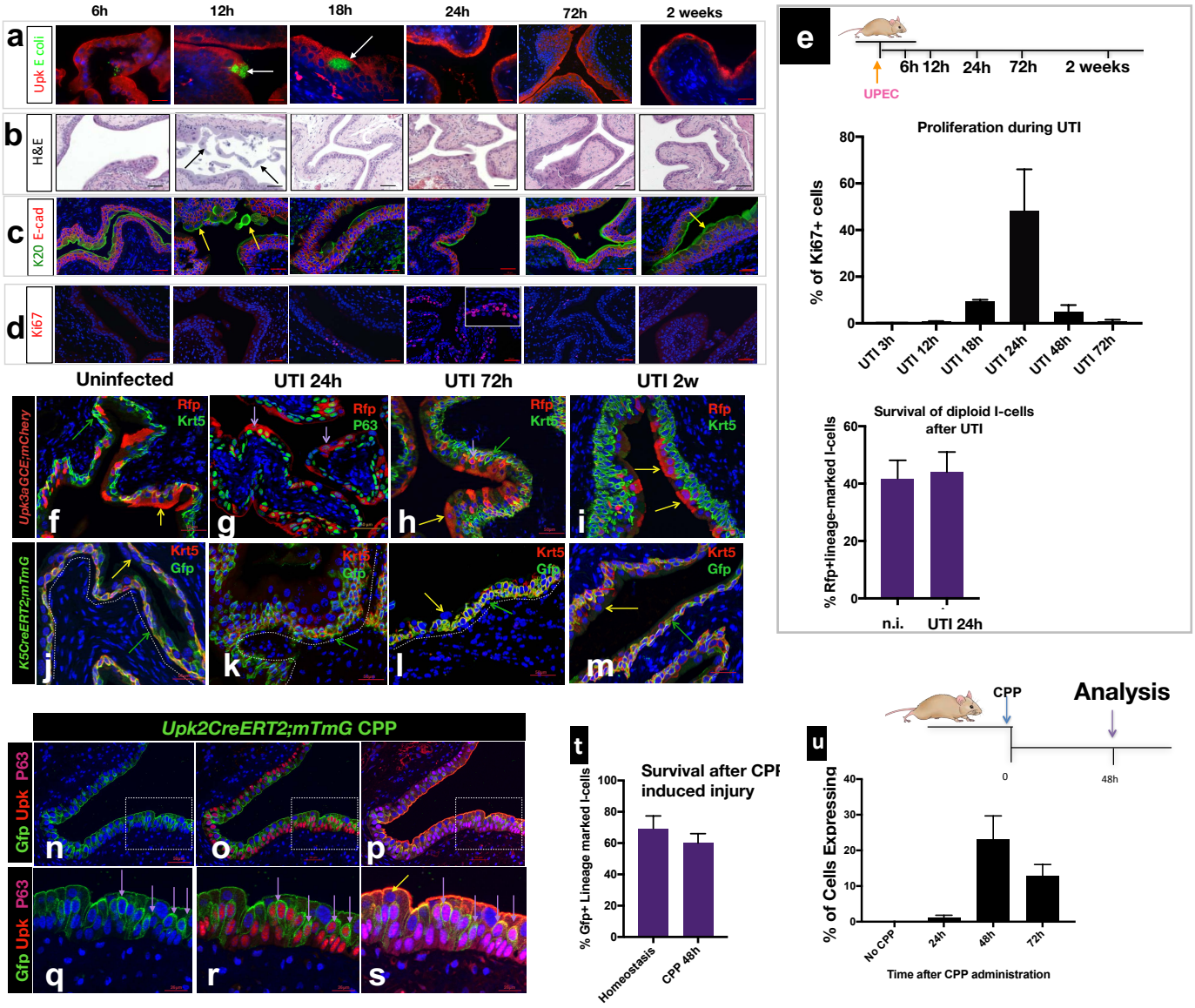

Figure S2. Models of injury and repair, related to Figure 2. (a) Animals were inoculated UPEC which invade S-cells initially produce intracellular bacterial communities (E.coli is stained green). **(b)** Invasion is followed by exfoliation (arrows). **(c)** The S-cell layer is replaced 72h after infection and the urothelial barrier is restored after 2 weeks. **(d)** Ki67 expression after UTI. **(e)** Graphs showing Ki67 expression at different times after UTI (left) and quantification of diploid I-cells in uninfected urothelium and in the urothelium 24h post-infection (right). **(f-i)** Lineage tracing I-cells in a UTI model of injury and repair. **(f)** A paraffin section from a Tm-induced adult *Upk3aGCE;mCherry* mouse that is uninfected, stained with P63 and Rfp. **(g)** A paraffin section from a *Upk3aGCE;mCherry* mouse 24h after infection, stained with P63 and Rfp. **(h)** A paraffin *Upk3aGCE;mCherry* mouse 72h p.i. stained for Krt5 and Rfp expression. **(i)** A paraffin section from a *Upk3aGCE;mCherry* mouse 2 weeks after infection, stained with Krt5 and Rfp. **(j)** A paraffin section from a *Krt5CreERT2;mTmG* mouse that is uninfected, stained with Krt5 and Gfp. **(k)** A paraffin section from a Tm-induced adult *Krt5CreERT2;mTmG* mouse 24h p.i., stained with Krt5 and Gfp. **(l)** A paraffin section from a Tm-induced adult *Krt5CreERT2;mTmG* mouse 72h p.i., stained with Krt5 and Gfp. **(m)** A paraffin section from *Krt5CreERT2;mTmG* mouse 2 weeks after infection, stained with Krt5 and Gfp. **(n-s)** Lineage tracing using the Upk2CreERT2;mTmG line in the CPP-induced model injury and regeneration. **(n)** Section from a *Upk2CreERT2;mTmG* mouse 48h after CPP stained for expression of Upk and Gfp. **(o)** Section from a *Upk2CreERT2;mTmG* mouse 48h after CPP stained for expression of Gfp and P63. **(p)** A section from a *Upk2CreERT2;mTmG* mouse 48h after CPP stained for expression of Gfp, Upk and P63. **(q)** Same sample as in **(n)** at a higher magnification. **(r)** Same sample as in **(o)** at a higher magnification. **(s)** Same section as in **(p)** at a higher magnification. **(t)** Bar graph showing the numbers of surviving I-cells after CPP. **(u)** Graph showing kinetics of proliferation after CPP. Scale bars: **(a,c)**: 25μm; **(b,d)** 50μm; **(f-m)**: 50μm; Scale bars **(n-p)** 50μm; **(q-s)** 25μm.

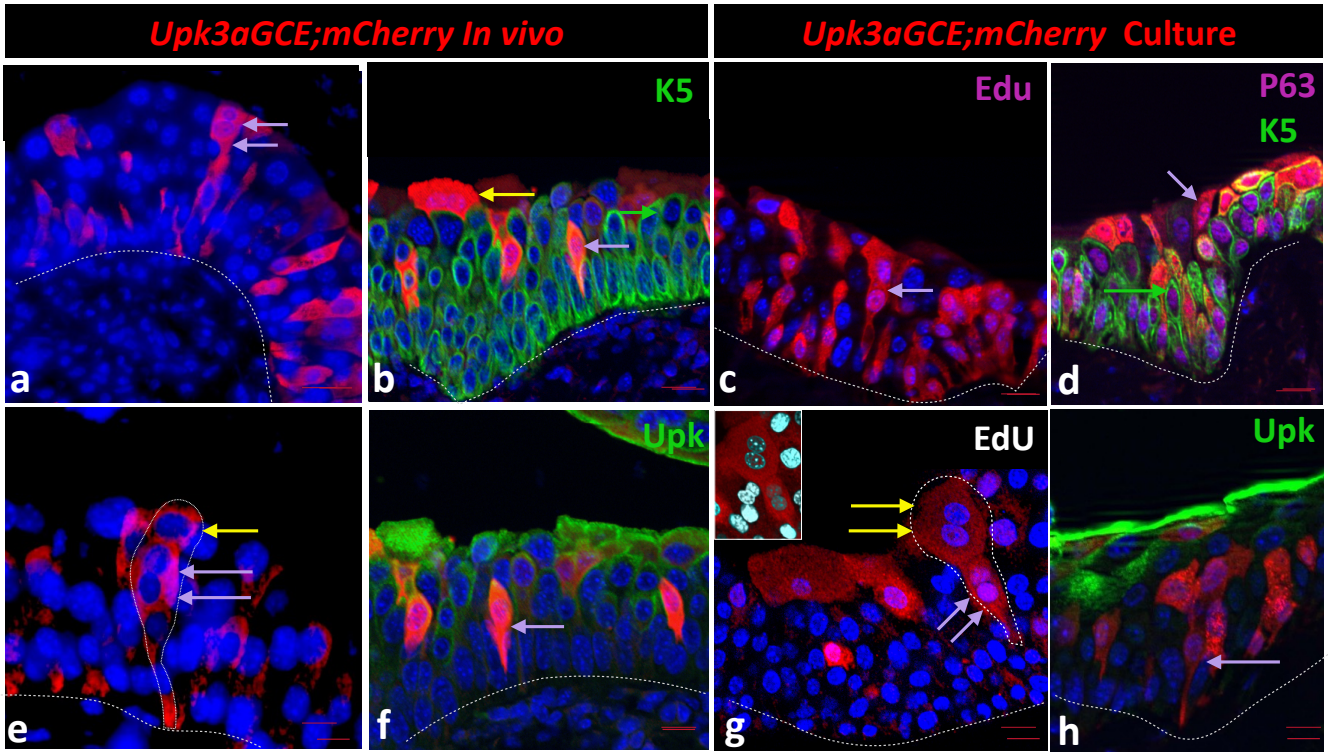

Figure S3. Comparison of in vivo regeneration and organotypic culture, related to Fig. 3. (**a)** Section from a *Upk3aGCE;mCherry* mouse 24h after UTI, stained for expression *mCherry.* Scale bar: 20mm. **(b)** A section from a *Upk3aGCE;mCherry* mouse 24h after UTI stained for expression of K5 and *mCherry*. **(c)** A section from an organotypic culture of urothelium and stroma isolated from a Tamoxifen-induced *Upk3aGCE;mCherry* mouse 4 days after plating, stained for expression of EdU and *mCherry*. Scale Bar: 20mm. **(d)** A section from an organotypic culture of urothelium and stroma isolated from a Tamoxifen-induced *Upk3aGCE;mCherry* mouse 4 days after plating, stained for expression of *mCherry,* P63 and K5. Scale Bar: 25mm **(e)** A Section from a *Upk3aGCE;mCherry* mouse bladder 24h after UTI, stained for *mCherry* expression. Scale bar: 20mm. **(f)** A Section from a *Upk3aGCE;mCherry* mouse bladder 24h after UTI, stained for *mCherry* and Upk expression. Scale bar: 20mm. **(g)** A section from an organotypic culture of urothelium and stroma isolated from a Tamoxifen-induced *Upk3aGCE;mCherry* mouse 4 days after plating, stained for expression of *mCherry* and P63. The inset shows EdU staining (white). Scale Bar: 20mm. **(h)** A section from an organotypic culture of urothelium and stroma isolated from a Tamoxifen-induced *Upk3aGCE;mCherry* mouse 4 days after plating, stained for expression of mCherry and Upk. Scale Bar:50 mm.